FOCCUS

Forecasting and observing the open-to-coastal ocean for Copernicus users

D5.4 Land-Ocean Continuum - Interfaces Report

WP5: Building, validation and demonstration of improved model interfaces in the Land-Ocean Continuum

30.07.2026/v1.0

Funded by the European Union

Funded by the European Union (Grant Agreement No. 101133911). Views and opinions expressed are however those of the author(s) only and do not necessarily reflect those of the European Union or the European Health and Digital Executive Agency (HaDEA). Neither the European Union nor the granting authority can be held responsible for them.

About this document

Title	D5.4 Land-Ocean Continuum - Interfaces Report
Work Package	WP5, Building, validation and demonstration of improved model interfaces in the Land-Ocean Continuum
Lead Partner	SMHI
Author(s)	Giorgia Verri (CMCC), Júlia Kaiser (CMCC), Fabio Viola (CMCC), Alessandro De Lorenzis (CMCC), Caterina Gianolla (CMCC), Vladimir Santos da Costa (CMCC), Alena Bartosova (SMHI), Francisco Campuzano (+ATLANTIC), Soraia Romão (+ATLANTIC), Pavel Terskii (SMHI), Olga Vigiak (CMCC, JRC), Lotta Beyaard (Deltares), Lorinc Meszaros (Deltares), Douglas Vieira da Silva (Hereon), Carolina Gramcianinov (Hereon), Benjamin Jacob (Hereon), Vilnis Frishfelds (DMI), Jun She (DMI)
Reviewers	Kelli Johnson (Hereon), Joanna Staneva (Hereon)
Due Date	31.07.2026, M31
Submission Date	31.07.2026
Version	**1.0**

Dissemination Level

X	PU: Public
	PP: Restricted to other programme participants (including the Commission)
	RE: Restricted to a group specified by the consortium (including the Commission)
	CO: Confidential, only for members of the consortium (including the Commission)

FOCCUS: Forecasting and observing the open-to-coastal ocean for Copernicus users is a Research and Innovation action (RIA) funded by the Horizon Europe Work programme topics addressed: HORIZON-CL4-2023-SPACE-01: Strategic autonomy in developing, deploying and using global space based infrastructures, services, applications and data 2023. Start date: 01 January 2024. End date: 31 December 2026.

Funded by the European Union

Funded by the European Union (Grant Agreement **No. 101133911**). Views and opinions expressed are however those of the author(s) only and do not necessarily reflect those of the European Union or the European Health and Digital Executive Agency (HaDEA). Neither the European Union nor the granting authority can be held responsible for them.

Table of Contents

1. Executive Summary 4
2. Analysis Of Seamless Modeling Techniques At The Land-Ocean Continuum 5
   2.1 Po River-Delta-Sea Continuum 5
   2.2 Tiber River-Delta-Sea Continuum 6
   2.3 Ofanto River-Estuary-Sea Continuum 8
   2.4 Danube River-Delta-Sea Continuum 11
   2.5 Tagus and Sado Rivers-Sea Continuum 15
      2.5.1 Sensitivity Analysis of Estuarine Geometry 19
   2.6. Randers Fjord Continuum 23
   2.7. German Bight River-Sea Continuum 28
   2.8. Northwestern Black Sea River-Sea Continuum 28
3. Analysis Of The Coupled Source to Sea Approaches 30
   3.1 Danube Delta and Black Sea 30
   3.2 Po and Ofanto with the Adriatic Sea 35
   3.3 Tagus and Sado Estuaries and the Portuguese Coast 48
   3.4 Dutch Continental Shelf 52
      3.4.1 Model Setup Differences 52
      3.4.2 Measurement Observations 53
      3.4.3 Model Performance Evaluation 54
      3.4.4 Other Benefits of E-HYPE 57
      3.4.5 Future Recommendations 57
   3.5 Northwestern Black Sea Coastal System 58
      3.5.1 Future Recommendations 60
   3.6 German Bight Coastal System 60
      3.6.1 Future Recommendations 63
   3.7 Danish Sea Coastal System 64
4. Conclusions 64
5. References 67
6. Annex 68

1. Executive Summary

The objective of WP5 is to assess and exploit the improvements in hydrological models and Land-ocean Continuum (LoC) interfaces (including the Estuary Emulator and the use of EMODnet near-real-time data) to enhance model-based monitoring and forecasting capabilities within the EU Copernicus Marine Service system. In this context, the present deliverable reports the advancements achieved in freshwater release representation through the activities carried out within Work Package (WP) 5 to optimize the LoC modeling interfaces. The following subtasks are included here:

- Judge the coupling and seamless modeling techniques at LoC interfaces;
- Contribute to advance the Copernicus Marine Service and Member State Coastal Systems (MSCS) via realistic freshwater release in terms of volume flux, active and passive tracers.

The evaluation and tuning of freshwater inputs were reported within Deliverable 5.1 (D5.1) along with a comparison of regional and continental-scale hydrological models, and with the datasets described in Deliverable 5.2 (D5.2). The validation of the dataset created to support the training phase of the Estuary Emulator (EE) using a high-resolution 3D finite element model (SHYFEM-MPI Z*) was reported in Deliverable 5.3 (D5.3). As part of the D5.3, the Milestone 5.1 (MS5.1, see Annex) describes the work setup and main achievements of the EE validation, and summarized the key findings and validation results of regional hydrological models (regional scale - MOHID-Land and WRF-Hydro; continental scale - HYPE and LISFLOOD+GREEN), providing conclusions about the particularities of implementation of the different hydrological models.

Therefore, the present document presents the modeling results obtained from the implementation of the improved LoC interfaces, connecting hydrological, coastal, and ocean models. To this end, the seamless modeling approach is analyzed for each case study, while the coupling framework is specifically evaluated for the a) Black Sea, considering Danube riverine inputs; b) the Adriatic Sea, considering the Po and Ofanto riverine contributions; c) the Portuguese coast, considering the Tago and Sado release; d) the Dutch Continental Shelf, considering both hydrological and biogeochemical inputs from E-HYPE; d) the Northwestern Black Sea, considering not only the hydrological and sediment input from E-HYPE for the major rivers, such as the Danube Delta and Dnister, but also for medium to small rivers in the domain; e) the German Bight, considering hydrological inputs for the main river systems Ems, Elbe and Weser and their associated tributaries; and f) Danish waters, where a two-way nested source-to-sea 3D modelling approach is applied to seamlessly resolve the fjord-estuary-coastal sea continuum with a resolution up to 50m. The reported results provide valuable support for advancing Copernicus Marine Services and MSCS within WP8 and WP9 (the integrated results will be detailed in the corresponding deliverables) through a more realistic representation of freshwater release, including volume fluxes, active and passive tracers, and sediment transport.

2. Analysis Of Seamless Modeling Techniques At The Land-Ocean Continuum

2.1 Po River-Delta-Sea Continuum

For creating the dataset that supports the EE designed to the Po Delta, as well as for the Tiber, Ofanto, and Danube regions, the model SHYFEM-MPI Z* was implemented based on a high resolution unstructured grid covering the entire river-sea continuum. All details on the computation mesh domains, time range of the simulations, and validation results were presented in D5.3. Considering the already validated methodology proposed for solving the connectivity between inland freshwater and marine saltwater at the LoC interfaces, representative flood and drought scenarios are presented to illustrate both the capability of the modeling approach to reproduce extreme events, and its ability to represent river plume dynamics under different environmental conditions.

Figure 2.1.1 presents maps of neural net Total Suspended Matter (TSM) derived from satellite imagery, compared with the 15 PSU and 32 PSU isohalines obtained from SHYFEM-MPI Z* simulations under high-discharge on November 26th 2019 (top panel) and low-discharge (bottom panel) conditions on July 31th 2022. As can be observed, the river plume represented by the model salinity fields is consistent with the TSM distribution derived from satellite data. During high-discharge events, the river plume extends several tens of kilometers offshore, transporting large amounts of suspended sediments seaward. In contrast, under low-discharge conditions, the influence of the Po Delta river plume is restricted to only a few kilometers around the river mouths, limiting the offshore transport of suspended sediments.

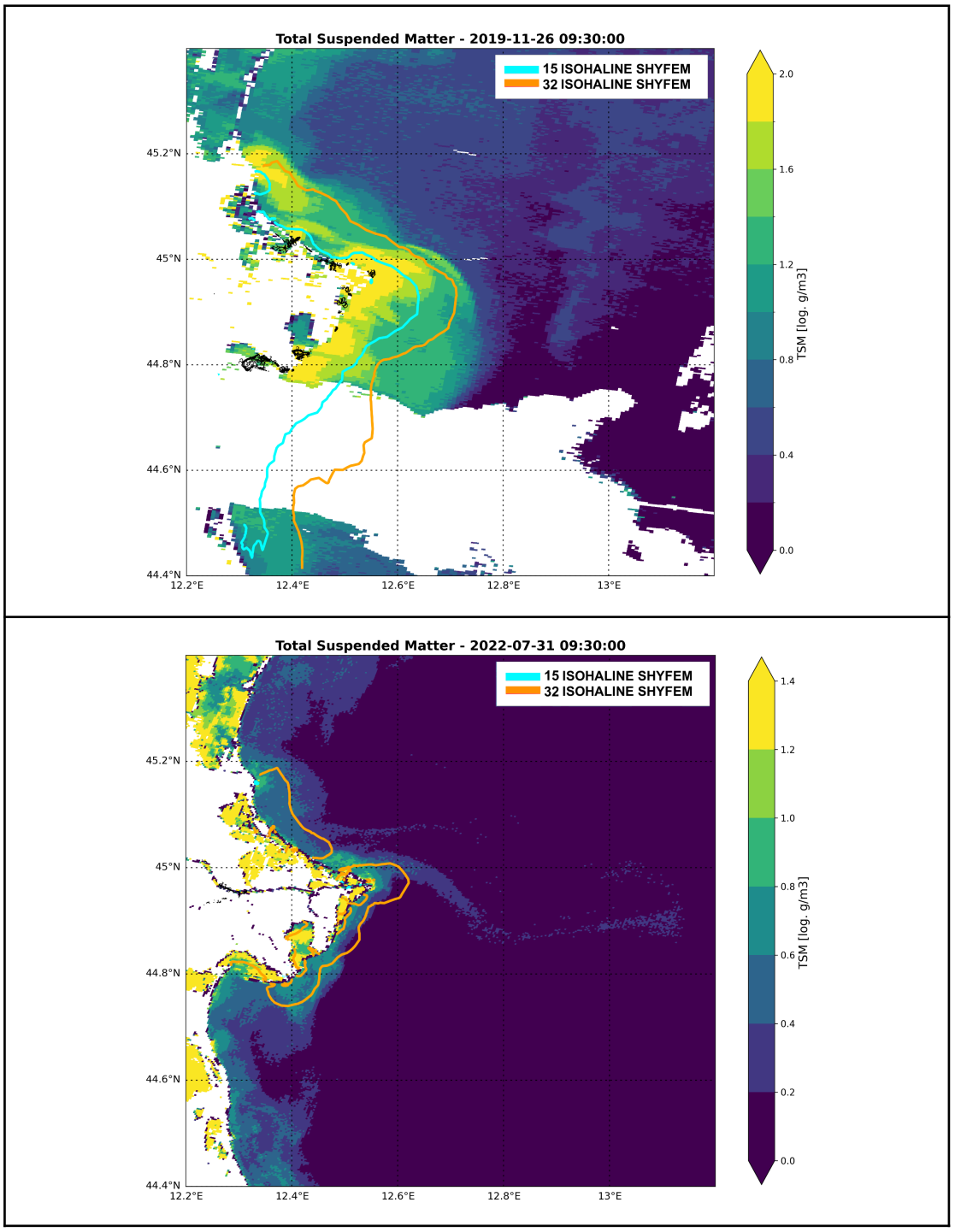


Figure 2.1.1 - Map of neural net TSM concentrations extracted from the sentinel-3 level-2 product for an event of high river discharge (top panel) and low river discharge (bottom panel). Isolines indicate contours of equal salinity (cyan: 15 PSU; orange: 32 PSU).

2.2 Tiber River-Delta-Sea Continuum

Figure 2.2.1 presents maps of TSM derived from satellite imagery for the Tiber coastal area, compared with the 25 PSU and 32 PSU isohalines obtained from SHYFEM-MPI Z* simulations under high-discharge (top panel) and low-discharge (bottom panel) conditions, specifically on December 14th 2020 and August 17th 2022, respectively. During high-discharge events, the Tiber River plume identified from the TSM data is consistent with the model salinity fields, indicating that the river influence extends significantly along the coastline. In these conditions, the freshwater contribution from the Fiumara Grande branch is clearly stronger than that from the Fiumicino branch. Under low-discharge conditions, however, the influence of the Tiber River plume becomes confined to the vicinity of the river mouths. Although the salinity field is still able to capture this behavior, the agreement with the TSM distribution is less evident, suggesting that, under reduced river discharge, other water properties may exert a stronger influence on the TSM signal.

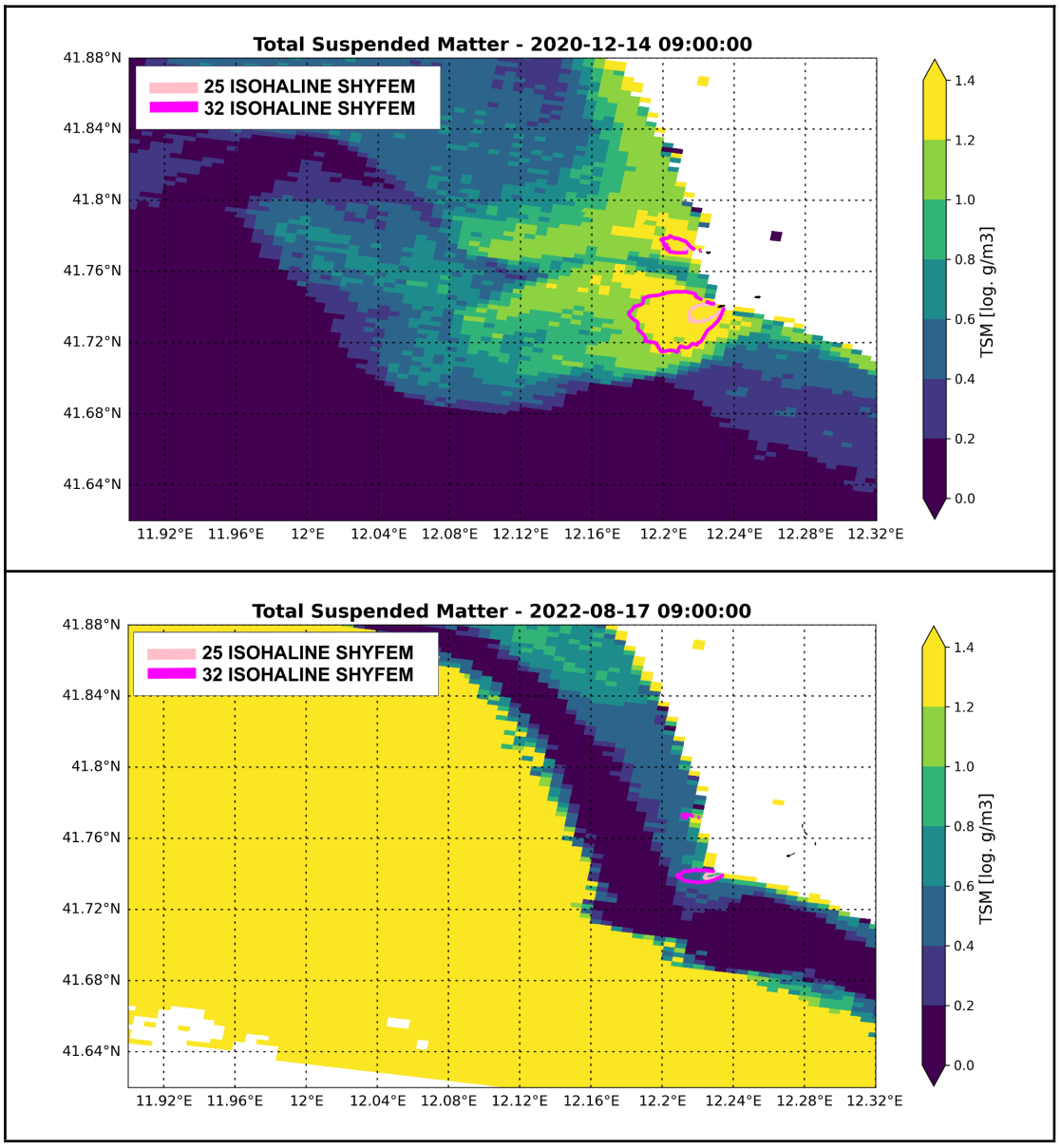


Figure 2.2.1 - Map of neural net TSM concentrations extracted from the sentinel-3 level-2 product for an event of high river discharge (top panel) and low river discharge (bottom panel). Isolines indicate contours of equal salinity (light pink: 25 PSU; magenta: 32 PSU).

2.3 Ofanto River-Estuary-Sea Continuum

Figure 2.3.1 presents maps of TSM derived from satellite imagery for the Ofanto coastal area, compared with the 36 PSU isohaline obtained from SHYFEM-MPI Z* simulations under

high-discharge (top panel) and low-discharge (bottom panel) conditions, specifically on January 13rd 2021 and November 30th 2019, respectively. Given the relatively small discharge of the Ofanto River compared to the other case studies, its influence on the coastal circulation is generally limited. During the dry season with low-flow conditions, the river plume is barely distinguishable along the coast. Even during low-discharge events, as shown in the bottom panel of Figure 2.3.1, the river influence remains confined to the immediate vicinity of the river mouth. Nevertheless, although infrequent in the region, high-discharge events can substantially enhance the extent of the river plume and its impact on the coastal zone. During the event of January 2021 (top panel of Figure 2.3.1), river discharge reached approximately 160 m^3/s on 11 January, representing a significant runoff event relative to the typical hydrological conditions of the Ofanto basin (for comparison, the low-flow event shown in the bottom panel was characterized by a river discharge of approximately 3 m^3/s). The offshore extension of the plume was well captured by the model and is supported by the TSM distribution derived from satellite imagery acquired two days later. It is worth noting that the contour plotted in Figure 2.3.1 corresponds to the 36 PSU isohaline, a substantially higher salinity threshold than those shown for the other case studies. Lower-salinity isohalines were not considered in the analysis because they remain confined to the riverine region, which is not adequately resolved in the satellite product because of its spatial resolution. This highlights the generally high salinity conditions of the area, even during periods influenced by river discharge. Although the river plume can extend some kilometers offshore during significant runoff events, its intensity remains relatively limited due to the modest freshwater input from the Ofanto catchment.

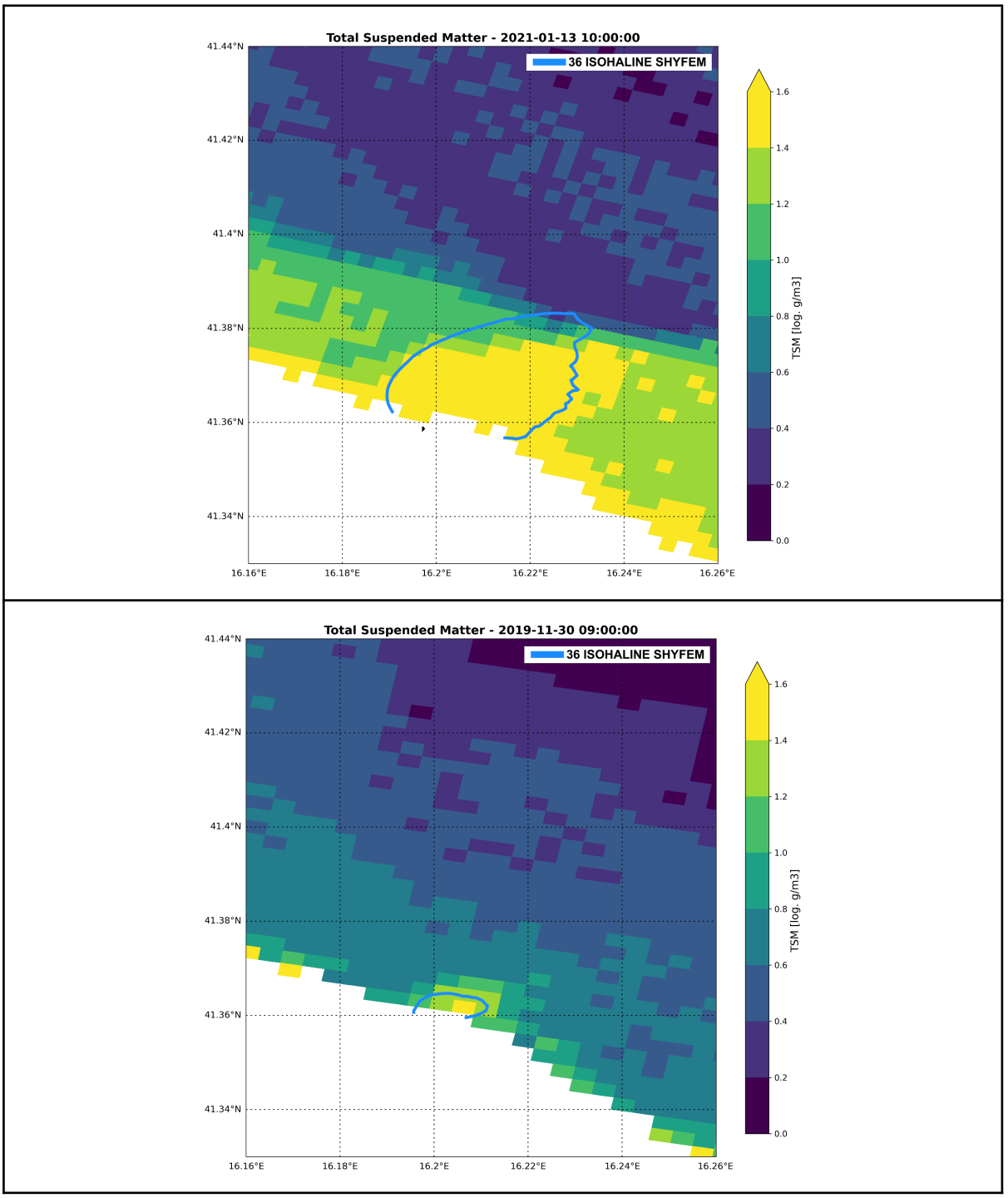
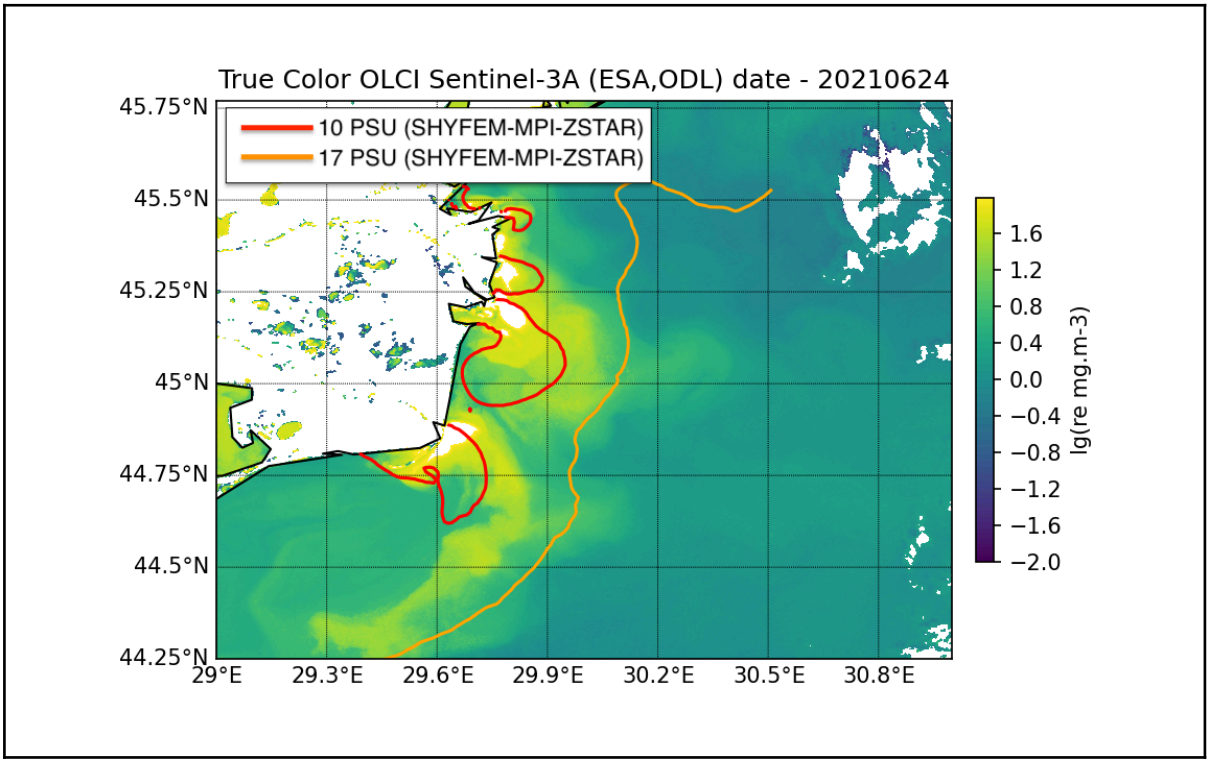


Figure 2.3.1 - Map of neural net TSM concentrations extracted from the sentinel-3 level-2 product for an event of high river discharge (top panel) and a moderate river discharge (bottom panel). The light blue isoline indicates the contour of 36 PSU.

2.4 Danube River-Delta-Sea Continuum

Figure 2.4.1 illustrates horizontal maps of TSM derived from satellite imagery within the Danube Delta region, with superimposed modeled isohalines at 10 PSU and 17 PSU obtained from the SHYFEM-MPI Z* simulations for two distinct runoff conditions: a high runoff event on June 24th 2021 (upper panel) and a low runoff event on November 22nd 2021 (lower panel). These maps clearly demonstrate that the model accurately reproduces both the shape and intensity of the plume. The 10 PSU isohaline closely aligns with regions of elevated TSM concentration, approximately 1.6 mg/m^3, during both high and low runoff conditions. Similarly, the 17 PSU isohaline corresponds qualitatively with a TSM patch near 1 mg/m^3 detected during the low runoff period.



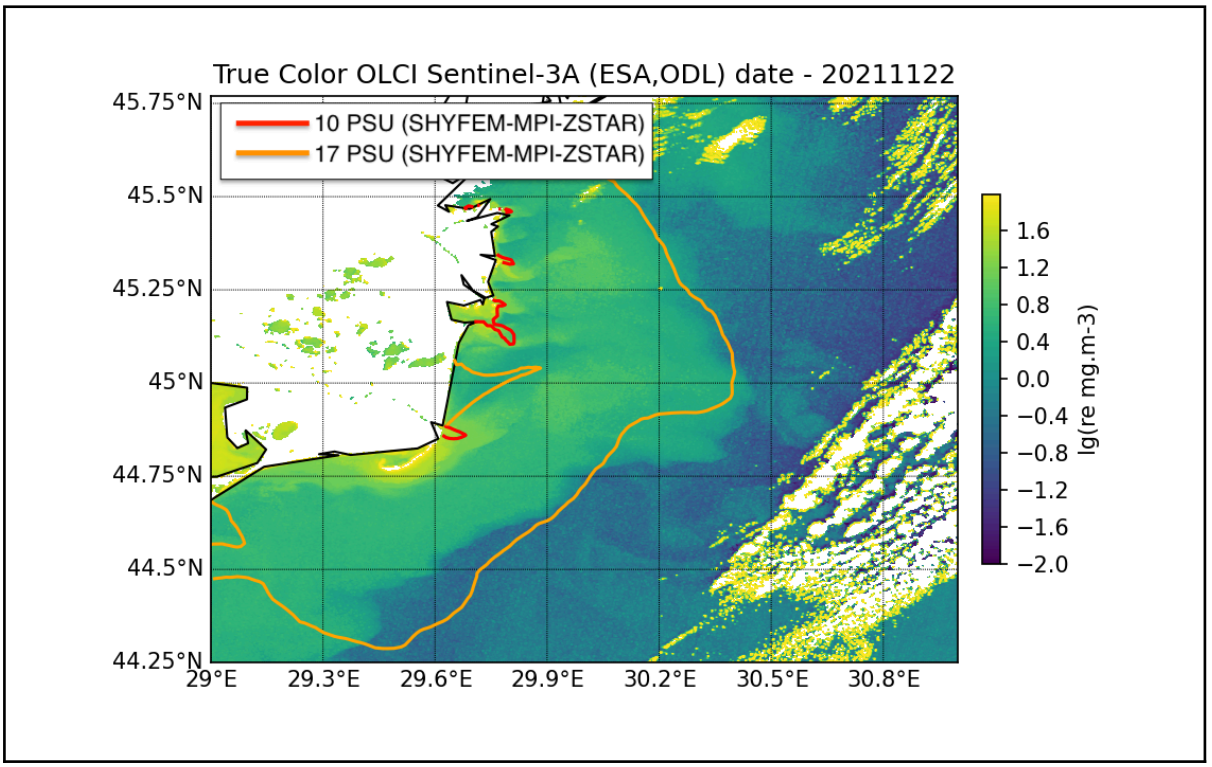


Figure 2.4.1 - Maps of TSM for a high runoff day (upper panel) and a low runoff day (lower panel). The overlapped red and orange lines are the modelled isohalines of 10 PSU and 17 PSU, respectively.

A twin experiment was conducted to assess the added value of prescribing river water temperature at an inland boundary of the Danube river-sea domain, located approximately 80 kilometers upstream from the coastline. The experiment, referred to as RiverR&S&T, involves the specification of river runoff, salinity, and temperature at the boundary nodes through surface boundary conditions. Given that the boundary is situated upstream of the estuarine zone, river salinity is set to zero. The river water temperature, on the other hand, is estimated using the Air2stream model (Toffolon et al., 2015). To isolate the influence of temperature prescription, a second simulation, named RiverR&S, was carried out under identical conditions but without imposing river temperature at the boundary.

Figure 2.4.2 shows two-dimensional (2D) maps of sea surface temperature (SST) for the spring (upper panel) and fall (lower panel) seasons considering the only Danube river-sea continuum. The experimental results highlight the crucial role of river temperature in accurately reproducing coastal dynamics. The impact of this thermal forcing undergoes a distinct seasonal inversion between spring and autumn. During the spring season, the river water acts as a cooling agent for the surrounding

marine environment, generating a distinct cold-water plume that extends along the coast and reduces the local sea surface temperature by more than 1°C compared SHYFEM EXP R&S. An opposite behavior is observed in the fall, where the river input introduces a warmer signal relative to SHYFEM EXP R&S, resulting in a positive thermal anomaly concentrated primarily near the delta outlets.

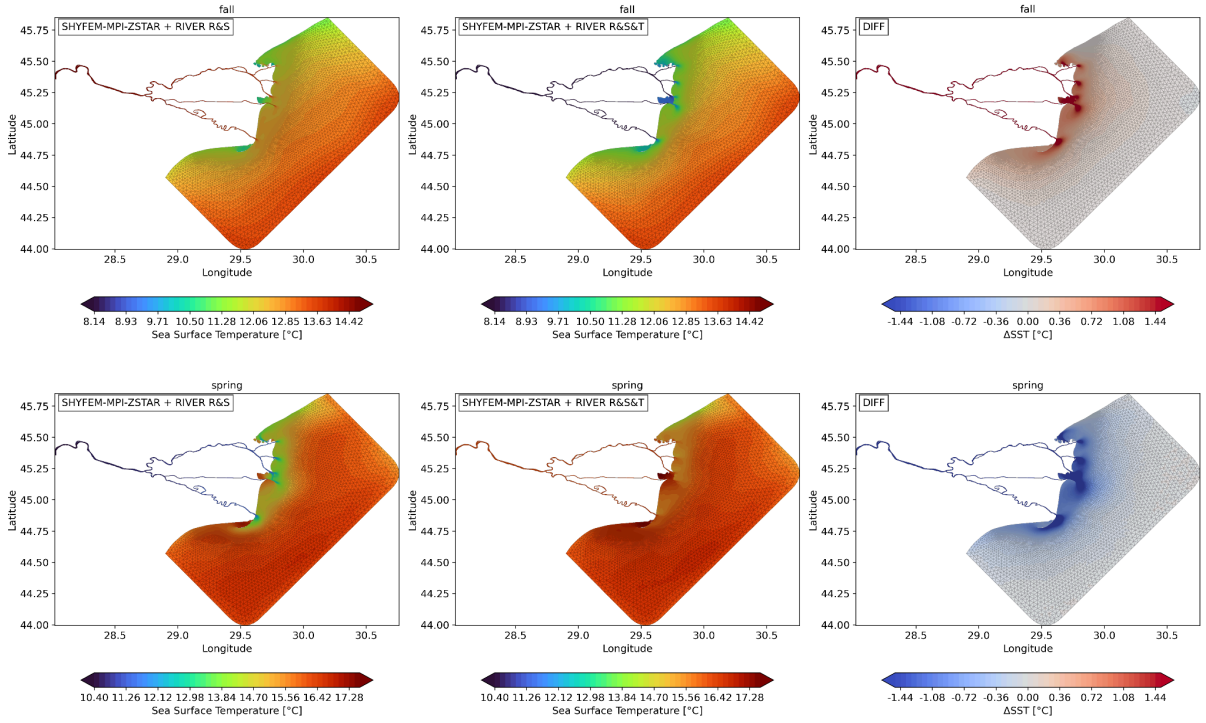


Figure 2.4.2 - Seasonal comparison of SST for spring (upper panel) and fall (lower panel). Left and middle panels show SST from the SHYFEM experiment without inland river temperature (R&S) and with inland river temperature (R&S&T), respectively. The right panel represents the temperature difference between the two simulations.

Figure 2.4.3 shows 2D maps of sea temperature at 20m depth for the spring (upper panel) and fall (lower panel) seasons considering the only Danube river-sea continuum. At a depth of 20 meters, the impact of the inland river temperature forcing becomes less important in both seasons. In spring, the difference between the two simulations is restricted to a minor offshore anomaly below 0.1°C, while in fall, the temperature fields are entirely identical, yielding a uniform 0°C difference across the domain. Furthermore, due to the bathymetry of the region, the shallowest coastal areas and river outlets do not extend to this depth. These results demonstrate that the thermodynamic influence of

the river freshwater plume is strongly stratified, remaining confined to the upper layers of the water column and failing to penetrate down to 20 meters depth.

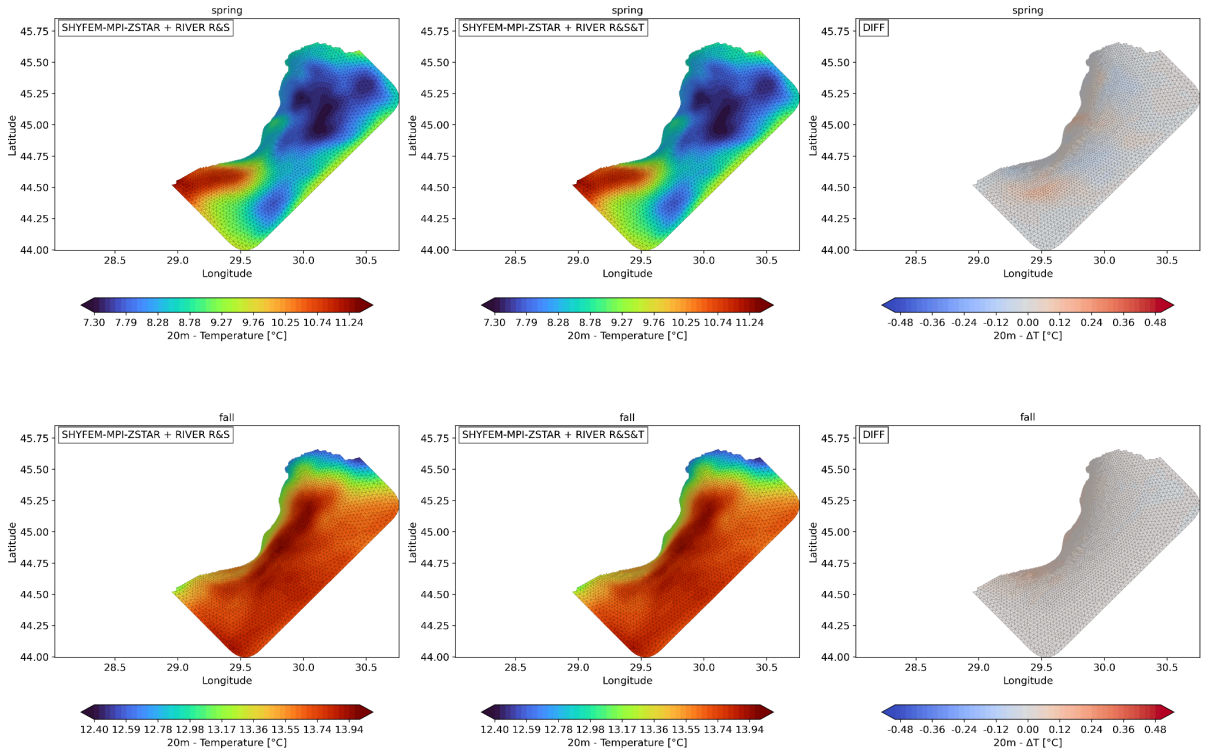


Figure 2.4.3 - Seasonal comparison of sea temperature at 20m depth for spring (upper panel) and fall (lower panel). The left and middle panels show sea temperature from the SHYFEM experiment without inland river temperature (R&S) and with inland river temperature (R&S&T), respectively. The right panel represents the temperature difference between the two simulations.

The Danube river-sea continuum was performed with SHYFEM-MPI Z* nested within Copernicus reanalysis products. This simulation produced a large and physically consistent learning dataset, which serves as a surrogate for in-situ observations, and is particularly valuable in the poorly monitored regions of the delta. The dataset enabled both training and testing of the EE, as its performance has been judged by comparison with available satellite observations. Figure 2.4.4 shows the validation of estuarine temperature and salinity at Chilia3, the mouth of Danube river. The machine learning (ML)-based EE closely reproduces the observed temperature at the mouth over the 1-year period considered, from April 2021 to April 2022. Concering salinity, no satellite observations were found. Nevertheless, it is possible to conclude that the EE performs as well as the learning 3D model used for its training.

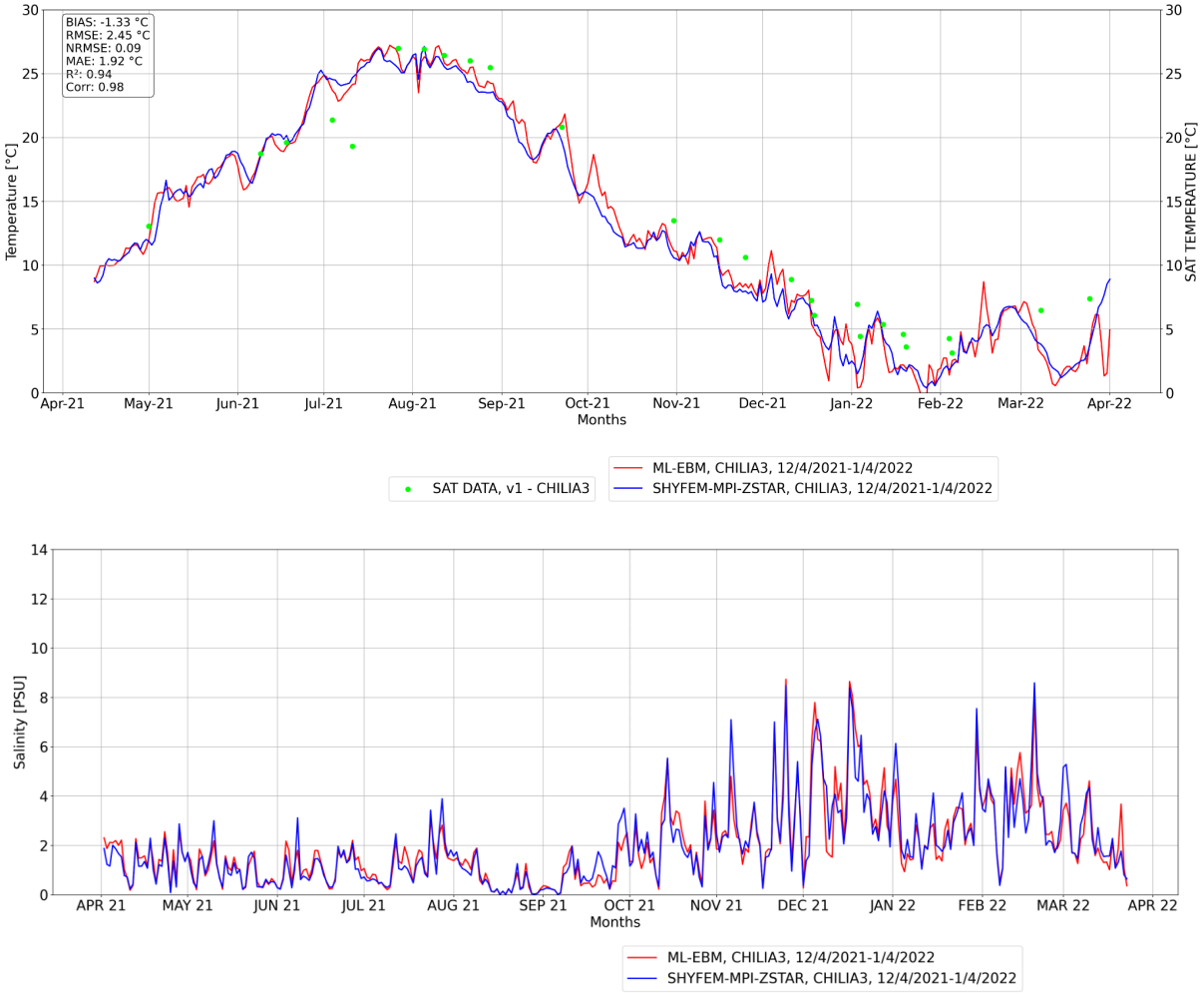


Figure 2.4.4 - Validation of the river temperature (upper panel) and river salinity (lower panel) of SHYFEM-MPI-ZSTAR (blue line) and ML-EBM (red line) for the Chilia3 branch with respect to satellite retrieved temperature (green dots).

2.5 Tagus and Sado Rivers-Sea Continuum

The previous EE framework was developed as a 2D model to reproduce the main hydrodynamic processes within estuarine systems, while maintaining a low computational cost suitable for operational applications. This section describes a 3D implementation of the EE to account for vertical variability and stratification processes. The 3D implementation incorporates the vertical structure of the water column, allowing the emulator to represent processes such as vertical salinity gradients, stratification and mixing processes, or depth-dependent circulation patterns.

The 3D implementation requires the definition of a vertical discretisation as well as the definition of vertical turbulence. The vertical discretisation includes a hybrid with near-surface discretisation, variable-thickness sigma layer with 12 levels, increasing from 1 m at the surface to 19.94 m in depth, above a layer with 63 z-levels increasing in thickness towards the bottom. Both EE implementations use river flow observations from the Portuguese Environmental Agency (APA) and those available at EMODnet, CMEMS Global Ocean 1/12° Physics Analysis and Forecast updated daily product in the ocean's open boundary, and GFS near real time data from NOAA as atmospheric forcing. The 2D implementation was presented in the performance assessment of the +Atlantic Estuarine Proxy Emulator in deliverable D5.3.

A comparison between the 2D implementation and the 3D version was performed using CoastNET observations, focusing on the emulator's ability to reproduce sea surface temperature and salinity. The time period analysed corresponds to the first three months of 2026 when severe weather conditions were registered in Portugal, with very deep low-pressure centres that brought strong winds, intense and persistent rains, and very energetic wave conditions. These weather conditions contributed to extreme river discharge episodes and flooding in some low-lying areas and river margins (Figure 2.5.1). In this analysis, only the Tagus Estuarine proxy is analysed, as no observational data are available for validation over the simulated period, and the discharge station used to force the model for the Sado Estuary became inoperative due to the extreme events that occurred in this period, preventing a reliable comparison for this EE.



Figure 2.5.1 - Tagus River flow at the Almourol station.

Figure 2.5.2 and Figure 2.5.3 compare the performance of the original 2D EE and the new 3D implementation against observations from the monitoring stations CN Buoy2 and CN Buoy3.

Temperature and salinity time series are presented together with the corresponding statistical indicators (Table 2.5.1), including bias, root mean square error (RMSE), skill score and Pearson correlation coefficient (r).

Overall, both model configurations reproduce the temporal variability of water temperature reasonably well. The seasonal warming observed during late February and early March are captured by both the 2D and 3D simulations, although differences are evident in the magnitude of the variability.

The 2D configuration systematically underestimates temperature at both buoys, with biases of −2.14 °C (Buoy2) and −1.93 °C (Buoy3). This bias is reflected in RMSE values of 2.64 °C and 2.47 °C, respectively. The 3D configuration substantially improves the representation of temperature at Buoy2, reducing the bias to −0.57 °C and the RMSE to 1.35 °C. At Buoy3, however, the improvement is less evident, with a bias of −1.68 °C and RMSE of 2.23 °C.

At Buoy2, the observations remain relatively stable while the simulated temperatures exhibit larger fluctuations, resulting in weaker correlations. The skill score is relatively low (0.24 – 0.46), indicating that although the seasonal evolution is reproduced, the models still have difficulty accurately representing short-term temperature variability.

For the salinity, the observed records show strong freshwater influence during late January and February, with salinity dropping to nearly 0 PSU, followed by a gradual recovery during March. This rapid transition reflects the extreme discharge events which occurred during January and early February. The 2D simulation reproduces the overall freshwater intrusion well. The gradual decrease from ocean conditions towards freshwater is consistent with observations, especially during January, when the model captures the progressive salinity reduction. This is reflected by relatively high correlation coefficients, 0.80 (Buoy2) and 0.66 (Buoy3). Despite this good temporal agreement, the model tends to overestimate salinity before the freshwater event, leading to positive biases of 2.01 PSU and 6.38 PSU, respectively. The larger RMSE values (9 – 12 PSU) mainly result from the strong salinity gradients occurring during the extreme events.

The 3D configuration shows worse performance for salinity. The model maintains salinity values mostly between 20 and 35 PSU, with only limited reductions during the simulation period with Bias reaching 18.20 PSU at Buoy2 and 11.78 PSU at Buoy3 and RMSE increases to 19.07 PSU and 14.01

PSU, respectively. Although the correlation coefficients remain moderately high (0.63–0.67), this mainly reflects that the model captures some timing of the variability rather than its magnitude.

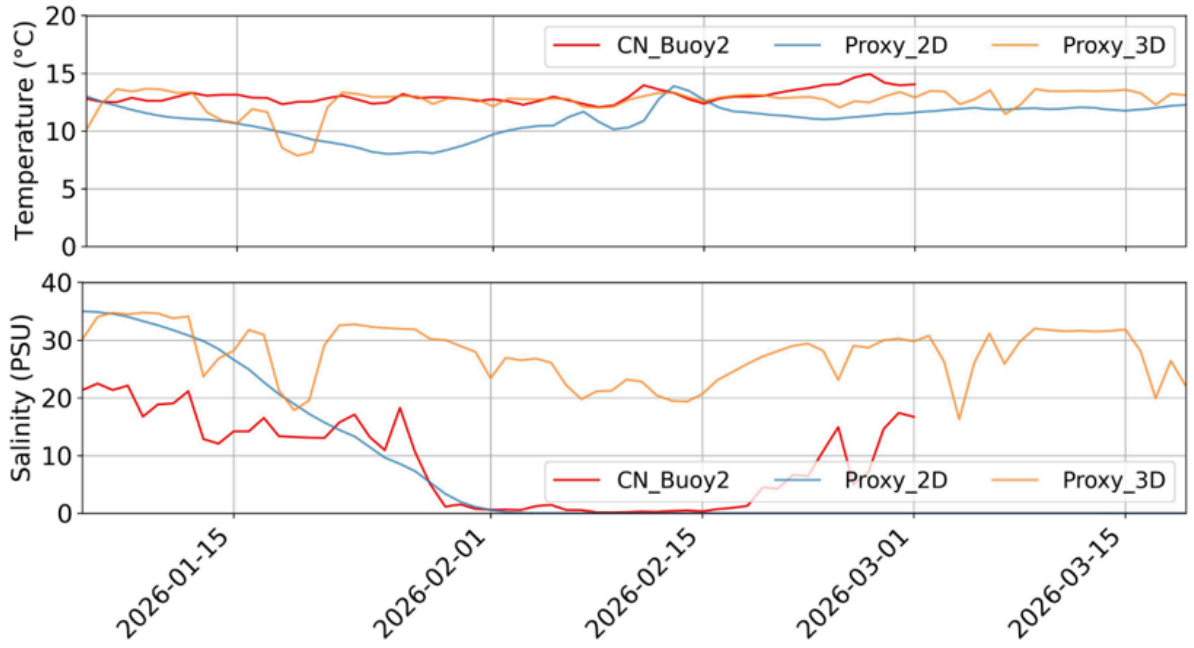


Figure 2.5.2 - Comparison of daily average temperature and salinity between CoastNET Buoy2 and 2D and 3D EE.

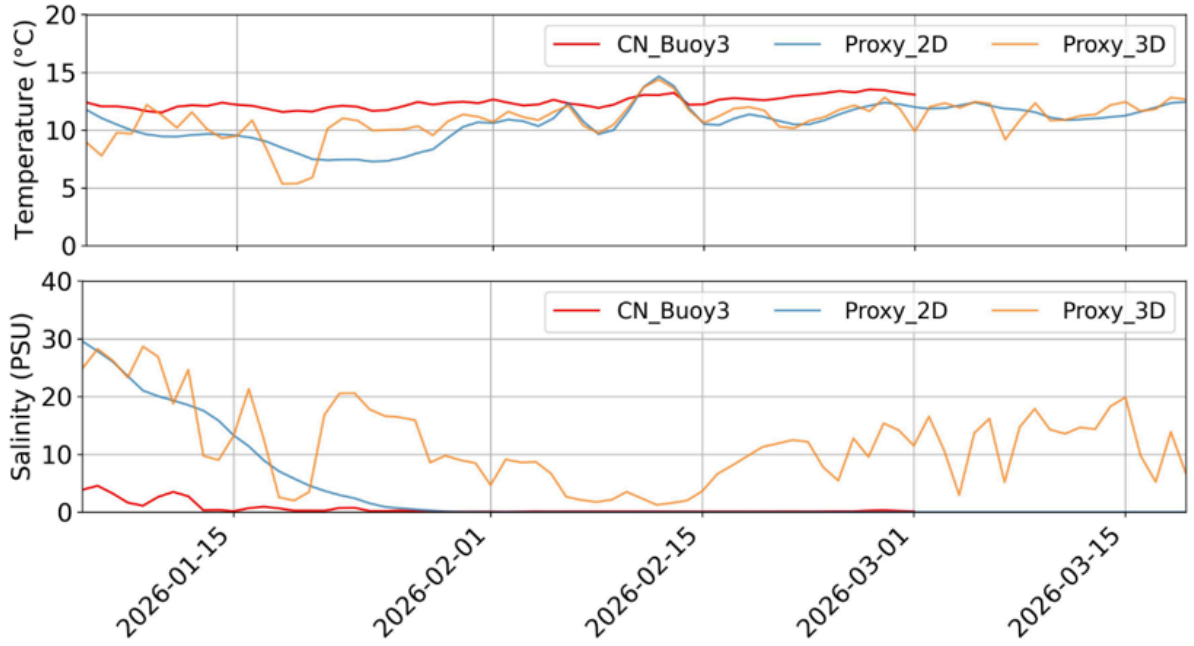


Figure 2.5.3 - Comparison of daily average temperature and salinity between CoastNET Buoy3 and 2D and 3D EE.

Table 2.5.1 - Statistical comparison between observed data and modelled outputs.

	Proxies 2D				***Proxies 3D***			
	Temperature		**Salinity**		**Temperature**		**Salinity**	
	Buoy2	**Buoy3**	**Buoy2**	**Buoy3**	**Buoy2**	**Buoy3**	**Buoy2**	**Buoy3**
BIAS	-2.14	-1.93	2.01	6.38	-0.57	-1.68	18.20	11.78
RMSE	2.64	2.47	9.17	12.11	1.35	2.23	19.07	14.01
SKILL	0.24	0.33	0.81	0.18	0.34	0.34	0.46	0.14
r	0.20	0.61	0.80	0.66	0.20	0.56	0.67	0.63

Overall, the results indicate that the transition to a 3D representation does not substantially modify the model skill for temperature simulations, suggesting that thermal dynamics are already adequately represented by the depth-averaged approach. However, the simplified 3D configuration does not adequately represent the freshwater intrusion reaching the buoy locations.

These results demonstrated that the main limitation of the original 3D implementation was associated with the estuarine representation rather than with the emulator methodology itself. The estuarine domain was excessively wide, allowing an unrealistically large intrusion of saline water from the ocean into the estuary. As a consequence, river freshwater inputs were rapidly diluted, resulting in salinity levels that were consistently higher than expected and a reduced representation of the estuarine salinity gradient.

2.5.1 Sensitivity Analysis of Estuarine Geometry

To improve the balance between freshwater inflow and marine intrusion, a set of experiments was performed using a reduced estuarine geometry, obtained by narrowing the effective estuarine width from 5 to 2 km. The objective was to improve the balance between oceanic intrusion and riverine forcing and to obtain a more realistic representation of mixing processes and salinity distribution within the estuary.

Figure 2.5.4 and Figure 2.5.5 present the comparison between observations, the operational 2D proxy, and the final 3D implementation using the reduced estuarine geometry, while Table 2.5.2 summarizes the corresponding performance indicators.

Comparing the 2D and 3D EE with the modified grid, both configurations reproduce the observed temperature variability reasonably well, with only minor differences. The 3D proxy slightly improves the performance at CN Buoy2, while both configurations show comparable results at CN Buoy3, with a systematic cold bias of approximately 2 – 2.5°C. The main improvements introduced by the 3D implementation are observed for salinity. At CN Buoy2, the 3D proxy substantially improves the representation of salinity dynamics, reducing RMSE from 9.60 to 5.84 PSU and increasing both skill (0.73 to 0.85) and correlation (0.60 to 0.78). Although salinity is slightly overestimated (+2.70 PSU), the temporal variability is reproduced more realistically than in the 2D configuration. The time series indicate that the 2D implementation rapidly converges towards unrealistically fresh conditions, particularly during periods of high river influence, whereas the 3D proxy maintains more realistic salinity gradients and better reproduces episodic saline intrusions (Figure 2.5.4).

Similar improvements are observed at CN Buoy3, where RMSE decreases from 7.40 to 4.04 PSU and the skill score increases from 0.14 to 0.35. Overall, the 3D implementation provides a more realistic representation of salinity dynamics and saline intrusion processes while maintaining comparable performance for temperature simulations.

The time series comparison clearly shows that the reduced geometry prevents the persistent marine dominance observed in the original configuration and allows the emulator to reproduce the observed alternation between freshwater influence and saline intrusion events.

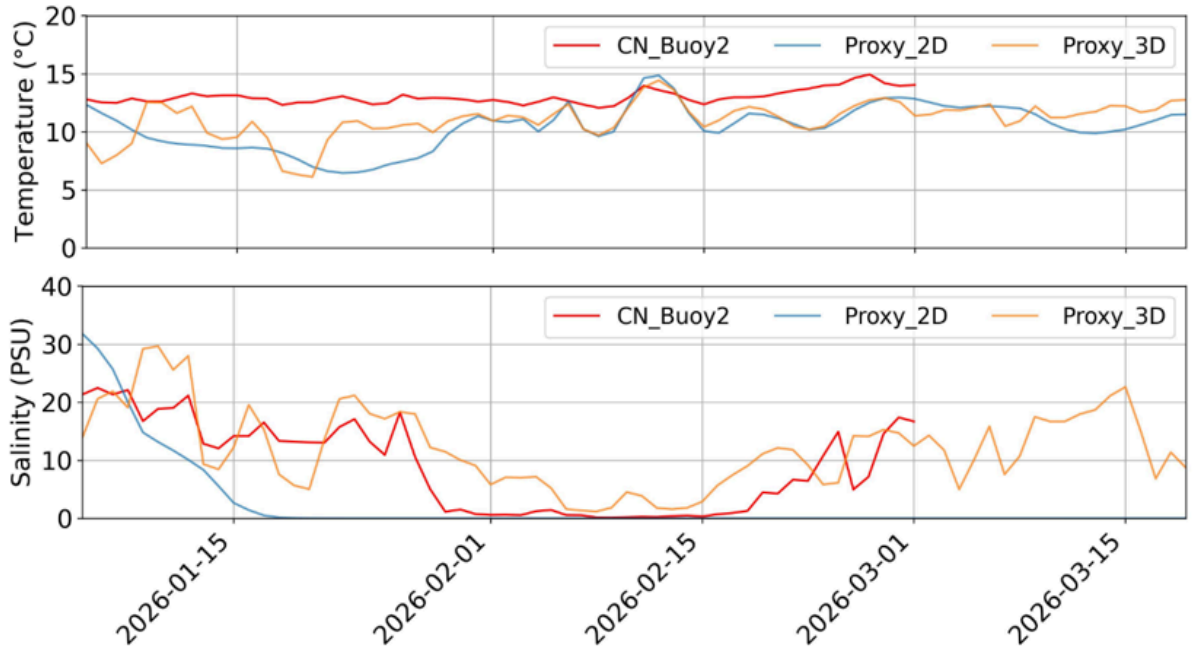


Figure 2.5.4 - Comparison of daily average temperature and salinity between CoastNET Buoy2 and 2D and 3D EE for the modified grid.

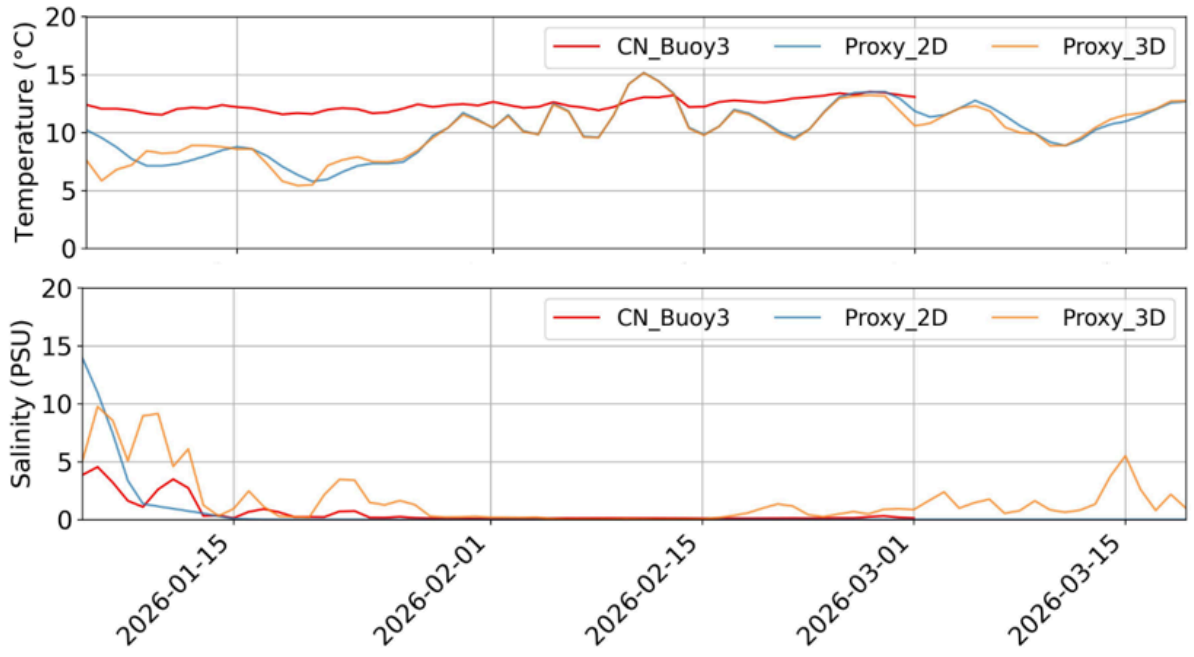


Figure 2.5.5 - Comparison of daily average temperature and salinity between CoastNET Buoy3 and 2D and 3D EE for the modified grid.

Table 2.5.2 - Statistical comparison between observed data and modelled outputs for the modified grid.

	Proxies 2D				***Proxies 3D***			
	Temperature		**Salinity**		**Temperature**		**Salinity**	
	Buoy2	**Buoy3**	**Buoy2**	**Buoy3**	**Buoy2**	**Buoy3**	**Buoy2**	**Buoy3**
BIAS	-2.61	-2.25	-4.23	1.92	-2.17	-2.52	2.70	1.70
RMSE	3.27	3.03	9.60	7.40	2.64	3.15	5.84	4.04
SKILL	0.23	0.32	0.73	0.14	0.28	0.30	0.85	0.35
r	0.41	0.75	0.60	0.26	0.45	0.78	0.78	0.48

When comparing the differences between the original and modified grid, in the case of temperature they were relatively small, indicating that thermal dynamics are less sensitive to estuarine geometry than salinity processes.

At CN_Buoy2, the reduced-grid 3D implementation decreased salinity RMSE from 19.07 PSU to 5.84 PSU and reduced the bias from 18.20 PSU to 2.70 PSU. The skill score increased from 0.46 to 0.85, while the correlation coefficient improved from 0.67 to 0.78. Similarly, at CN_Buoy3, salinity RMSE decreased from 14.01 PSU to 4.04 PSU, while bias was reduced from 11.78 PSU to 1.70 PSU. The skill score increased from 0.14 to 0.35, although the correlation coefficient decreased slightly from 0.63 to 0.48, suggesting that while the timing of individual salinity events was not always accurately reproduced, the overall magnitude and variability of salinity conditions were substantially improved (Table 2.5.1 and Table 2.5.2).

The sensitivity analysis demonstrated that estuarine geometry, particularly the representation of a realistic estuary mouth width, exerts a strong control on salinity patterns and stratification processes. The original geometry resulted in excessive saltwater intrusion and unrealistic dilution of riverine freshwater inputs, whereas the adjusted geometry reduced the penetration of saline water and improved freshwater retention within the estuary. This led to a more realistic representation of estuarine circulation and salinity dynamics in both the 2D and 3D implementations.

Overall, the reduced-grid 3D configuration represents a significant improvement over both the original 2D and 3D implementations for salinity simulations, while maintaining comparable performance for temperature predictions.

In contrast to salinity, temperature simulations appear to be relatively insensitive to both model dimensionality and estuarine geometry. The best agreement with observations is generally observed during periods of reduced river influence, while larger discrepancies occur during high river discharge events. This behaviour suggests that uncertainties in the prescribed river temperature forcing may represent one of the main sources of error in both the 2D and 3D implementations, independently of the estuarine geometry adopted.

2.6. Randers Fjord Continuum

There exist many river-fjord-open sea systems in Danish waters. Randers Fjord represents a typical case of such systems. Randers Fjord (Fig. 2.6.1) is connected to Kattegat and thus is part of the North Sea - Baltic Sea system. The western part of the Randers Fjord up to Randers city is very narrow as a river or channel. The fjord is used also for shipping up to Randers, therefore the fjord - river system is well connected to the Kattegat.

In the current DMI operational forecasting system, the Randers Fjord is covered by the inner Danish domain with a horizontal resolution of 0.5 nautical miles (nm), which cannot sufficiently resolve the river-fjord-open sea interaction. In FOCCUS, we applied the on-demand ocean model HBMos (Frishfelds et al., 2025) to model the area. HBMos was developed in the EU project EDITO-Model Lab, and can easily make new high resolution setups with a two-way nested solution. For the Randers Fjord continuum setup, the fjord itself is resolved in 50 m horizontal resolution, which is connected to Kattegat with 185 m horizontal resolution. The Kattegat domain is two-way nested in inner Danish waters with a resolution of 0.5 nm, which is two-way nested to the North Sea and the Baltic Sea. The vertical resolution is 1 or 2 meters in Randers Fjord. The first setup was made with publicly available bathymetry of Randers Fjord. The setup was run for the period of July 2023-October 2024 using DMI Harmonie weather forcing of 2.5 km resolution. It was found that the bathymetry (Fig. 2.6.1) was not deep enough. Therefore, the Randers Fjord bathymetry was deepened by using shipping line information. With this bathymetry an “extended setup” was made, and was run for the period of January 2020 - December 2023. There are two rivers included in the Randers Fjord domain: Gudenå river, with yearly average runoff 33 m3/s, and the small Alling river, with just over 1 m3/s runoff. The river discharge is taken according to the E-HYPE hydrological model.

The model simulations were validated using observations at three stations (Fig. 2.6.2) for surface salinity and temperature. Results are shown in Fig. 2.6.3 - Fig. 2.6.5, respectively. While SST is

dominated by a strong seasonal variation, surface salinity shows significant intra- and interannual variability, as well as spatial variability. It is expected that rivers have great impacts on the surface salinity. The model reproduces SST quite well, and also the highs and lows of salinity at both stations, although some of the observed amplitudes were underestimated. The results also show that the salinity from the simulation with deepened bathymetry is fresher than the undeepened one.

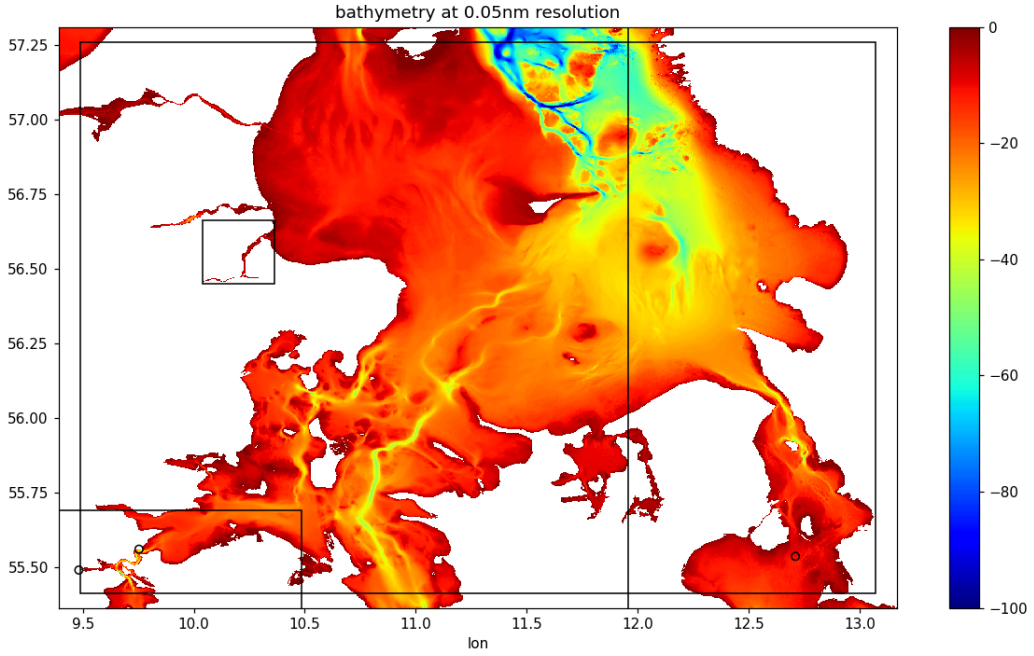


Figure 2.6.1 - Layout of Kattegat and Randers Fjord domains.

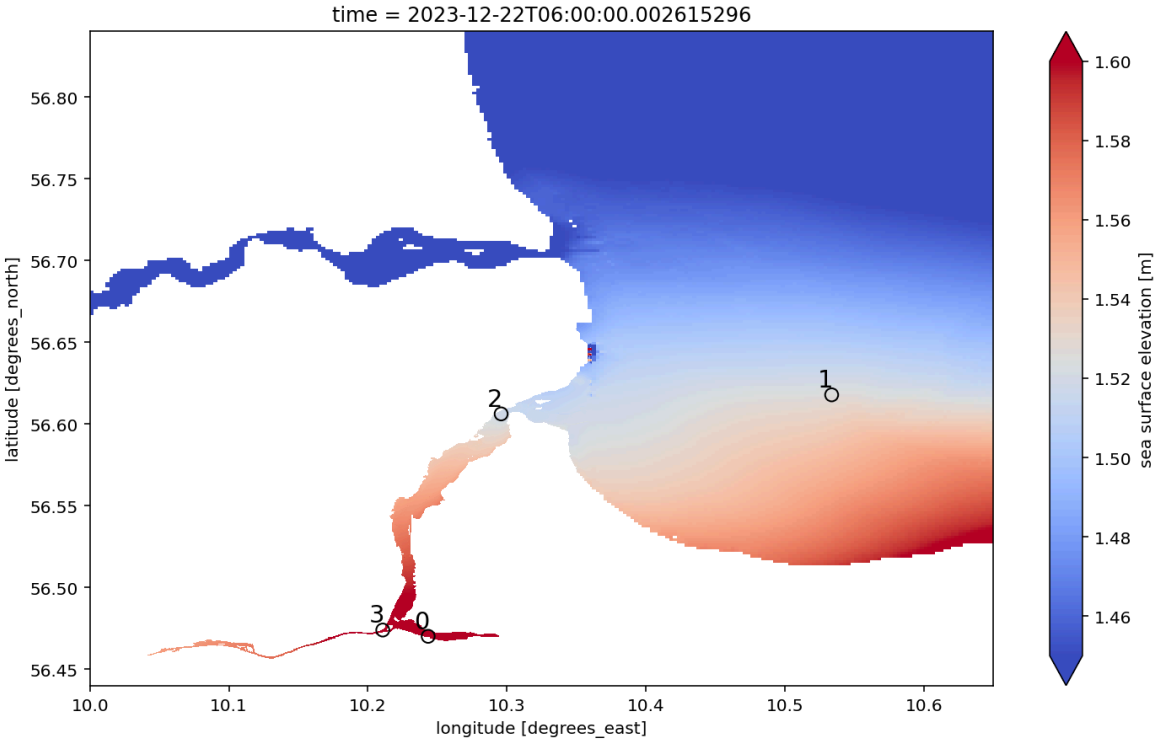


Figure 2.6.2 - Randers Fjord is located in the southwestern area. There are 3 locations with salinity/temperature profile observations and one location east from the fjord.

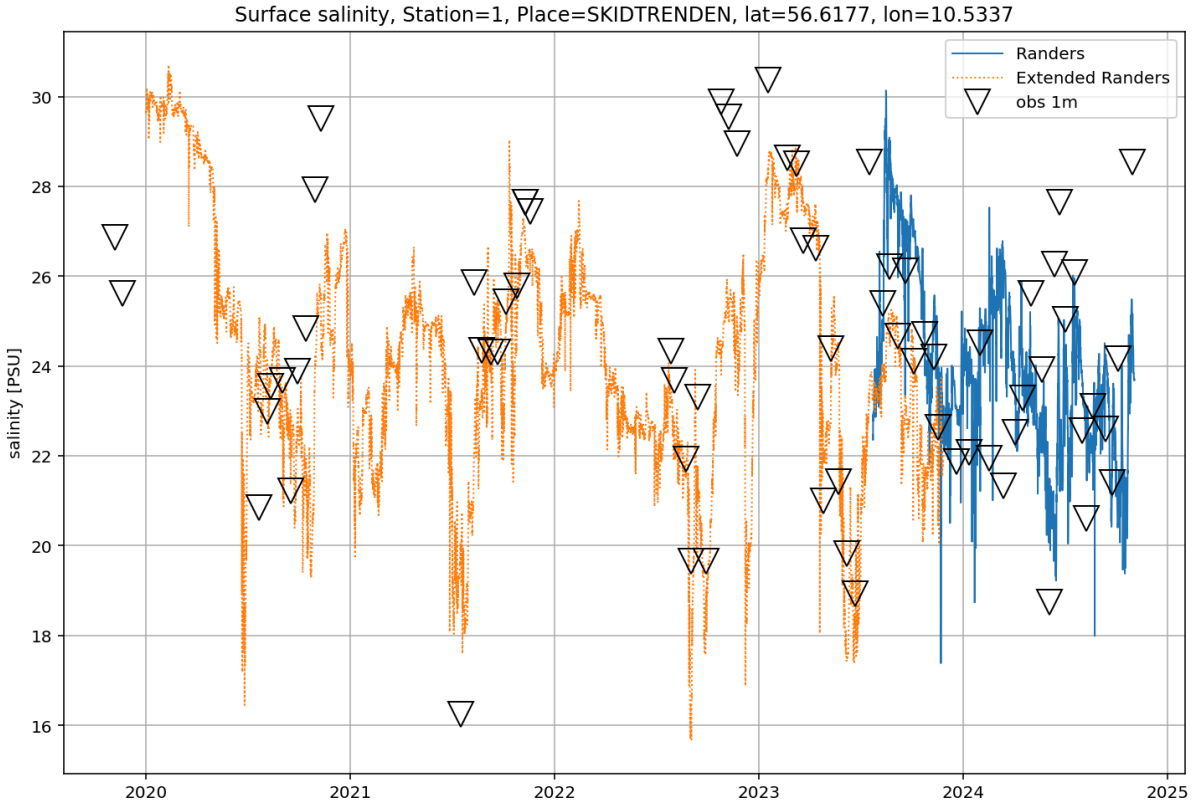


Figure 2.6.3 - Simulated sea surface salinity with (orange) and without (blue) bathymetry deepening against observations at 1 m depth at Station 1 (offshore).

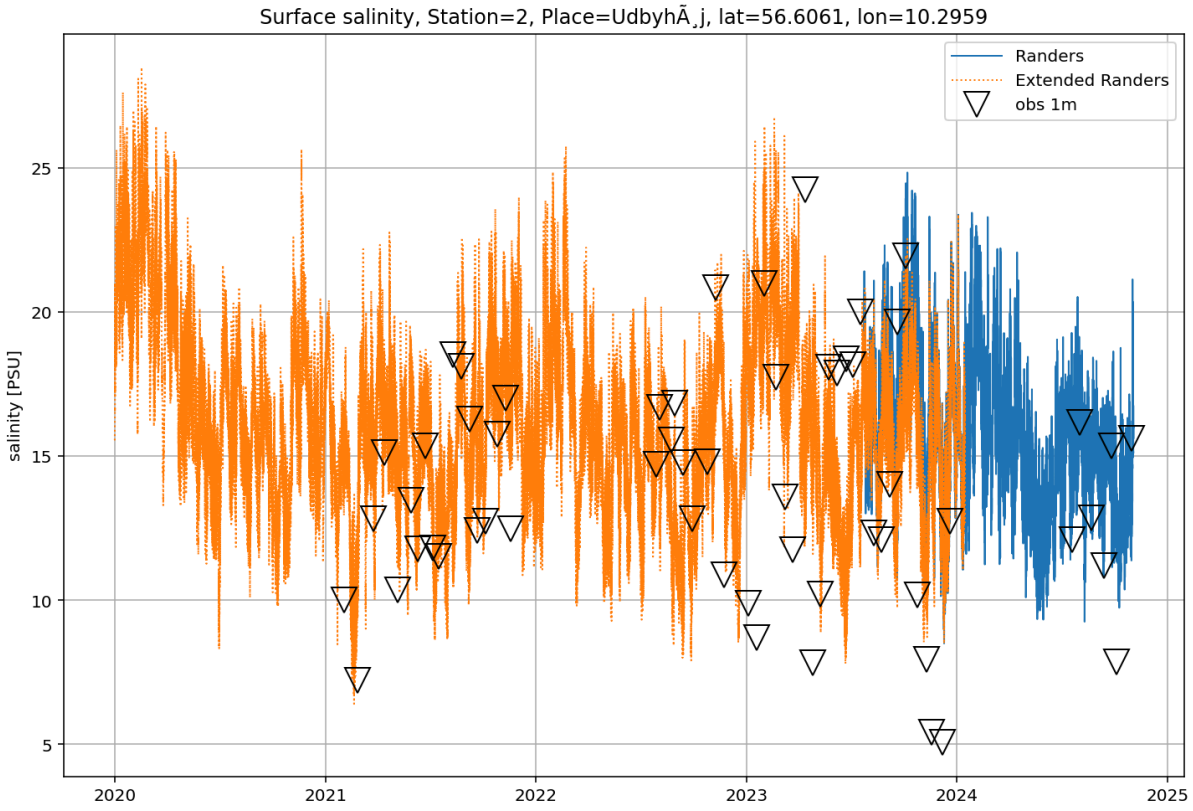


Figure 2.6.4 - Simulated sea surface salinity with (orange) and without (blue) bathymetry deepening against observations at 1 m depth at Station 2 (exit of the fjord)

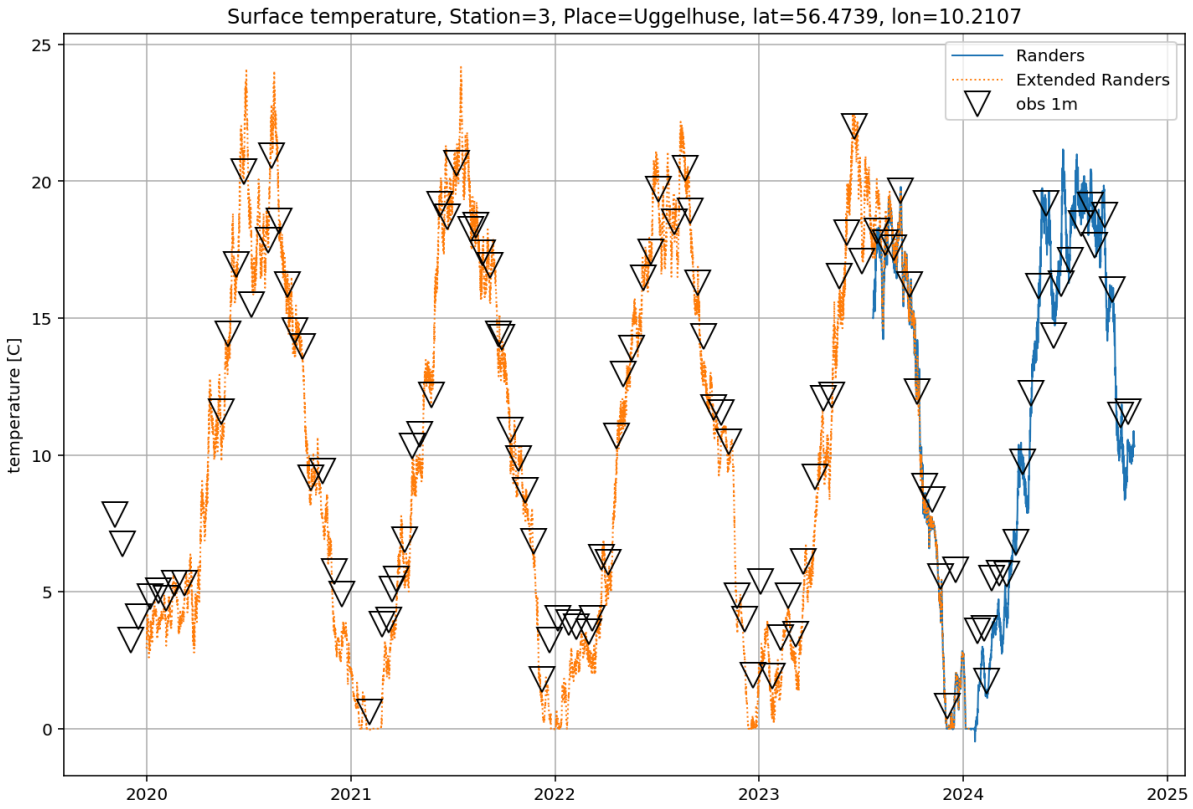


Figure 2.6.5 - Simulated sea surface temperature with (orange) and without (blue) bathymetry deepening against observations at 1 m depth at Station 3 (entrance of the fjord)

2.7. German Bight River-Sea Continuum

The representation of the river-sea continuum for the German Bight had been introduced in the GCOAST-GB setup using results from the E-HYPE model (MS4.1; D5.2). Thereby, the contribution of the small rivers and tributaries was included in GCOAST-GB that prior utilised historical data for the major river systems of the Weser, Elbe, as well as the Eider. An assessment of the results using salinity as a prognostic variable was presented in section 2.3 of the D5.3 report. One key result is the partial improvement of the RMSE, especially due to a reduced bias for the coastal station in the Elbe (the largest contributor) river mouth area (station Cuxhaven). In section 3.6, the validation is now expanded.

2.8. Northwestern Black Sea River-Sea Continuum

The Northwestern Black Sea river–sea continuum setup has been extended to explicitly include the Danube Delta distributary branches. Although previous deliverables primarily reported the added

value of coupling the GCOAST-BS model with E-HYPE, this extended configuration comes with a substantially higher computational cost. Consequently, long-term simulations are limited, and this section focuses on presenting the model setup.

The river–sea continuum configuration is shown in Figure 2.9.1. The domain includes the Danube distributary branches and extends upstream to Ceatal Izmail. By explicitly representing the river network connected to the open sea, the setup provides a more consistent interface with watershed models and hydrological monitoring stations. It also improves the estimation of discharge partitioning among the individual distributary branches, as the flow distribution is dynamically determined through the process-based interaction between sea level variations and mass fluxes across the open boundaries.

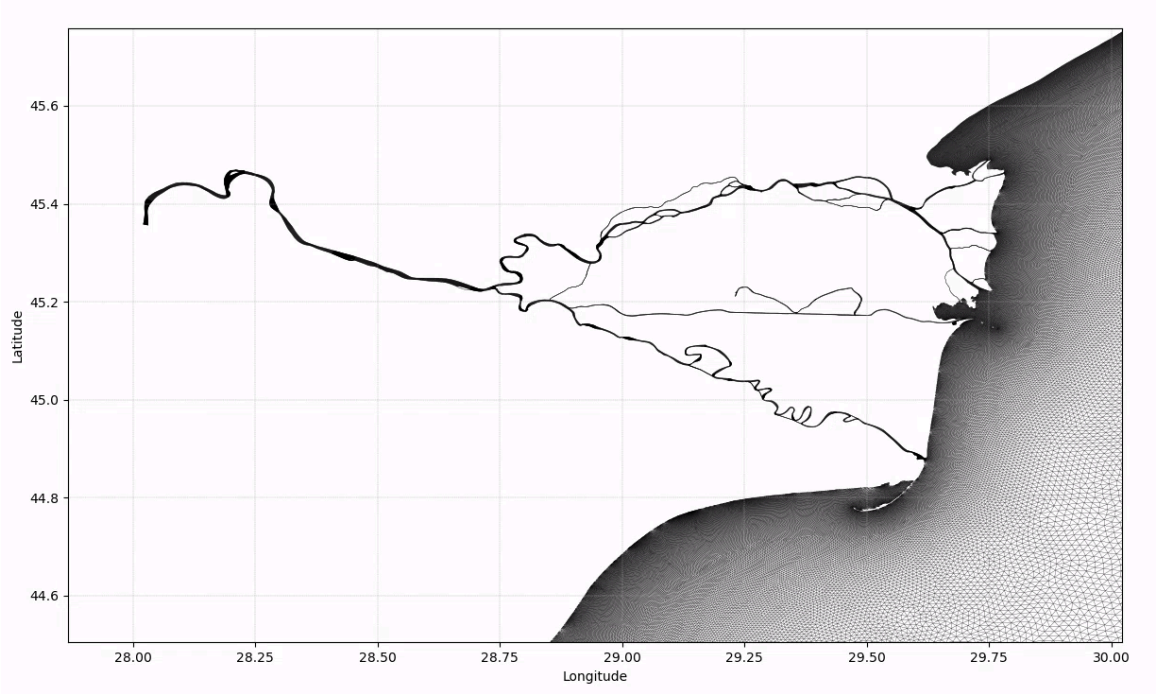


Figure 2.9.1 - Model setup for the Northwestern Black Sea river–sea continuum, including the Danube River and its distributary branches connected to the open sea.

The extended setup reproduces the spatial gradients across the Danube Delta, providing enhanced capabilities for seamless LoC applications. Figure 2.9.2 presents the simulated sea surface salinity field, demonstrating the model's ability to resolve salinity gradients within the distributary network and their connectivity with the adjacent coastal ocean. Future developments will incorporate the improvements achieved within GCOAST-BS under WP5 into this extended river–sea continuum configuration.

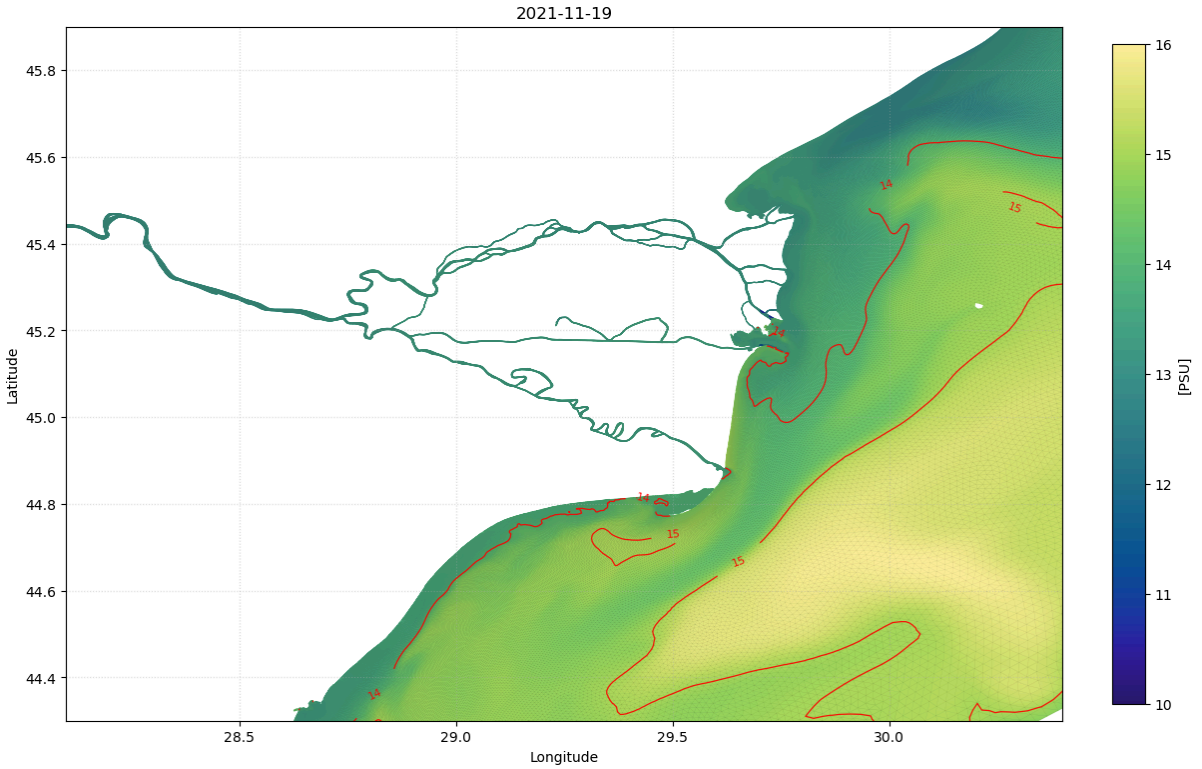


Figure 2.9.2 - Simulated sea surface salinity field illustrating the river-sea salinity gradients across the Danube Delta and the adjacent Northwestern Black Sea.

3. Analysis Of The Coupled Source to Sea Approaches

3.1 Danube Delta and Black Sea

The objective is to evaluate the ability of the Black Sea regional NEMO model to represent the Danube river plume when forced with more realistic river boundary conditions from the EE. Multi-annual sensitivity experiments (2019-2021) compare simulations using observed or climatological river inputs upstream of the delta with EE-derived discharge, salinity, and temperature prescribed at the river mouths, accounting for hydrodynamic transformations within the delta. For that, we are considering a) the Control Run as a stand-alone, multi-annual historical simulation forced at the river mouths, with daily observed river discharge and monthly climatological salinity, where river temperature is not included; b) the Sensitivity Run 1, an offline two-way coupled simulation in which the climatological and observed river boundary conditions are replaced by river discharge and salinity estimated by the EE, forced by the Control Run, and provided at the river mouths on a daily basis; and c) Sensitivity Run 2, which further includes the river temperature provided by the EE. In the offline two-way coupling framework, the EE is forced by the Control Run

ocean conditions together with observed river discharge, zero river salinity, and river temperature estimated by the Air2stream model. The resulting river discharge, salinity, and temperature at the river mouths are then used as surface boundary conditions in the NEMO sensitivity experiments.

Figure 3.1.1 and 3.1.2 highlight how the SHYFEM model, thanks to its high-resolution unstructured mesh, explicitly resolves the river delta channels and simulates sharp, localized freshwater plumes directly at the river mouths. Conversely, the NEMO runs rely on a coarser, pixelated coastline. Within the NEMO configurations, the Control Run displays a highly diffused and smoother freshwater plume along the coast, whereas Sensitivity Run 1 and 2 capture a much fresher, distinct core (< 4 PSU) localized near the main river outlets, an effect that remains consistent across both summer and winter seasons.

In the maximum runoff scenario (Figure 3.1.3), the freshwater signals (0−5 PSU) are drastically amplified across all simulations, making the structural differences between the models even more relevant. This figure demonstrates that, while the coarser regular grid of the NEMO simulations smooths the coastal area, the high-resolution SHYFEM model explicitly resolves the complex geometry of the Danube's branches and its offshore area, capturing the outflowing brackish water, which is especially relevant in the case of high runoff.

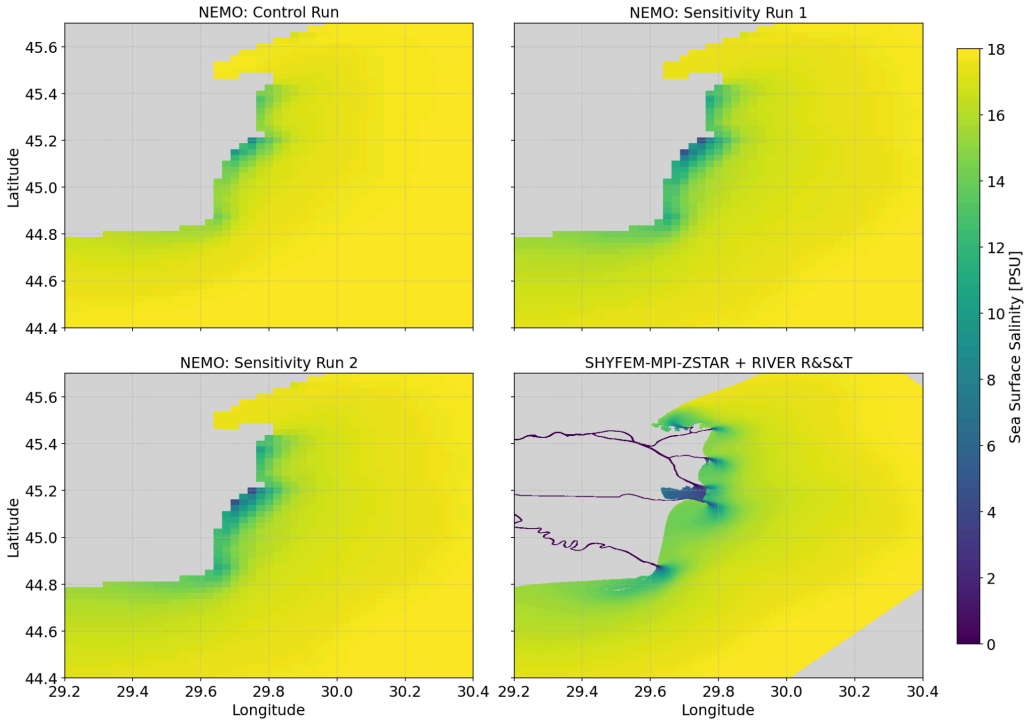


Figure 3.1.1 - Comparison of Sea Surface Salinity (SSS) simulated by NEMO (Control Run, Sensitivity Run 1, and Sensitivity Run 2) and SHYFEM-MPI-ZSTAR + RIVER R&S&T models during the winter season.

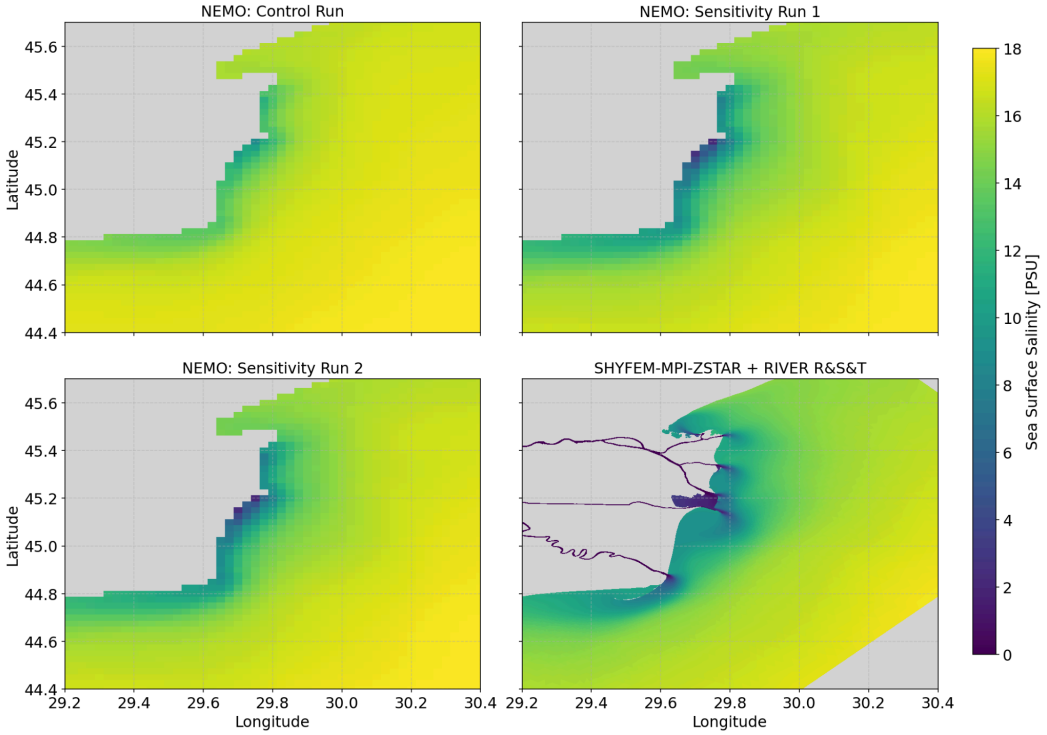


Figure 3.1.2 - Comparison of Sea Surface Salinity (SSS) simulated by NEMO (Control Run, Sensitivity Run 1, and Sensitivity Run 2) and SHYFEM-MPI-ZSTAR + RIVER R&S&T models during the summer season.

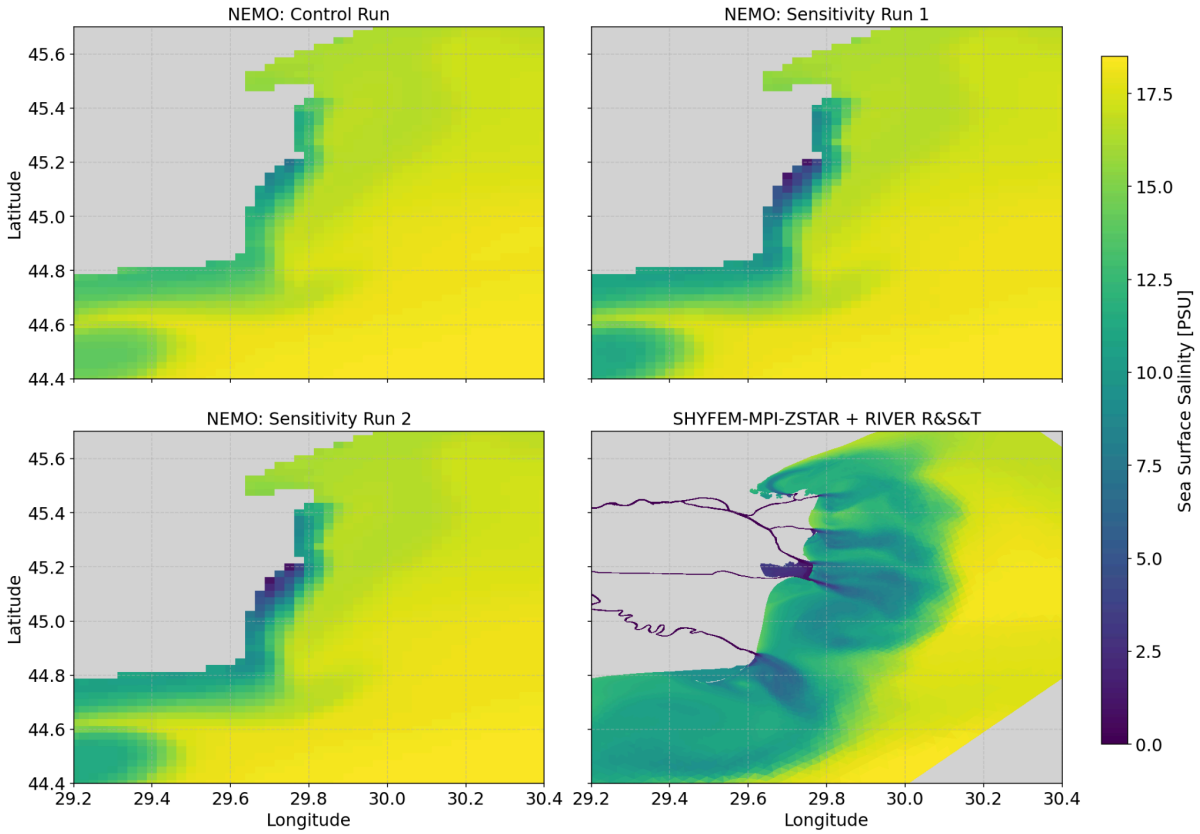


Figure 3.1.3 - Comparison of Sea Surface Salinity (SSS) simulated by NEMO (Control Run, Sensitivity Run 1, and Sensitivity Run 2) and SHYFEM-MPI-ZSTAR + RIVER R&S&T models during the highest runoff day.

At a depth of 20 meters (Figure 3.1.3 and 3.1.4), the differences between the configurations become more subtle, with salinity values operating within a much narrower, higher marine range (17.2–18.6 PSU). The SHYFEM model stands out drastically from NEMO, displaying a distinct, localized high-salinity core (> 18.2 PSU) near the coast around latitude in summer, and a sharp, confined low-salinity channel pushing offshore in winter. Within the NEMO suite, the differences are subtle: the Control Run shows a smoother, more uniform salinity distribution across the basin, whereas Sensitivity Runs 1 and 2 successfully capture a stronger pool of fresher water (<17 PSU) trapped along the southern boundary, showing almost identical subsurface patterns to each other.

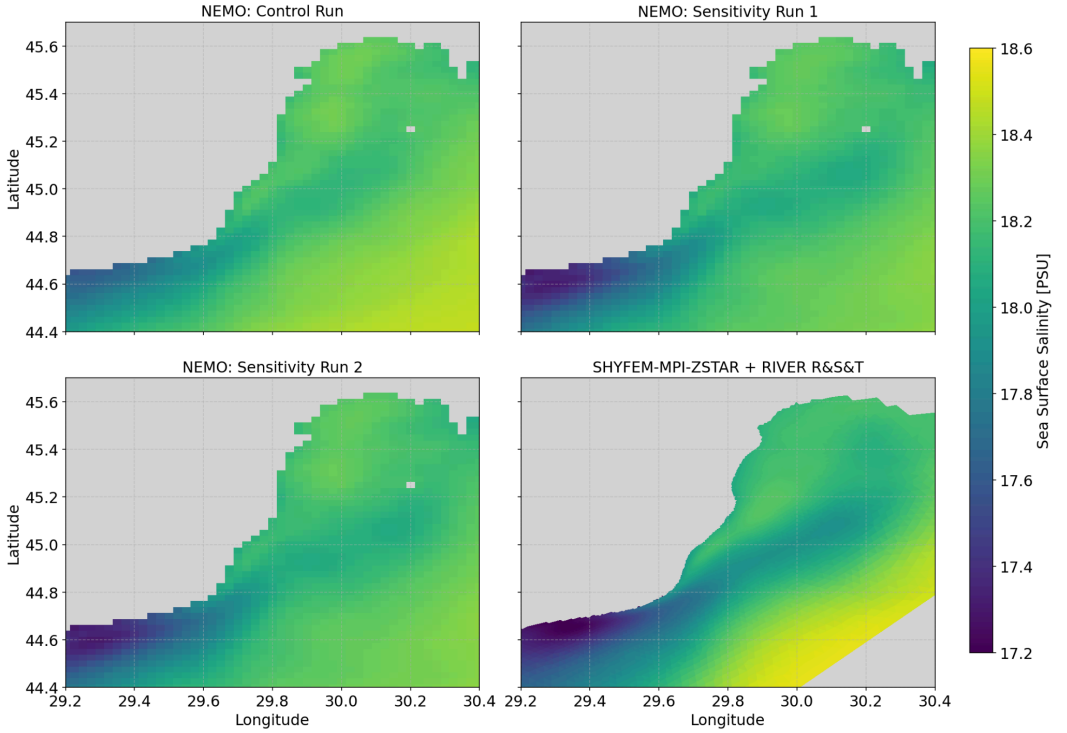


Figure 3.1.3 - Comparison of Sea Salinity at 20m depth simulated by NEMO (Control Run, Sensitivity Run 1, and Sensitivity Run 2) and SHYFEM-MPI-ZSTAR + RIVER R&S&T models during the winter season.

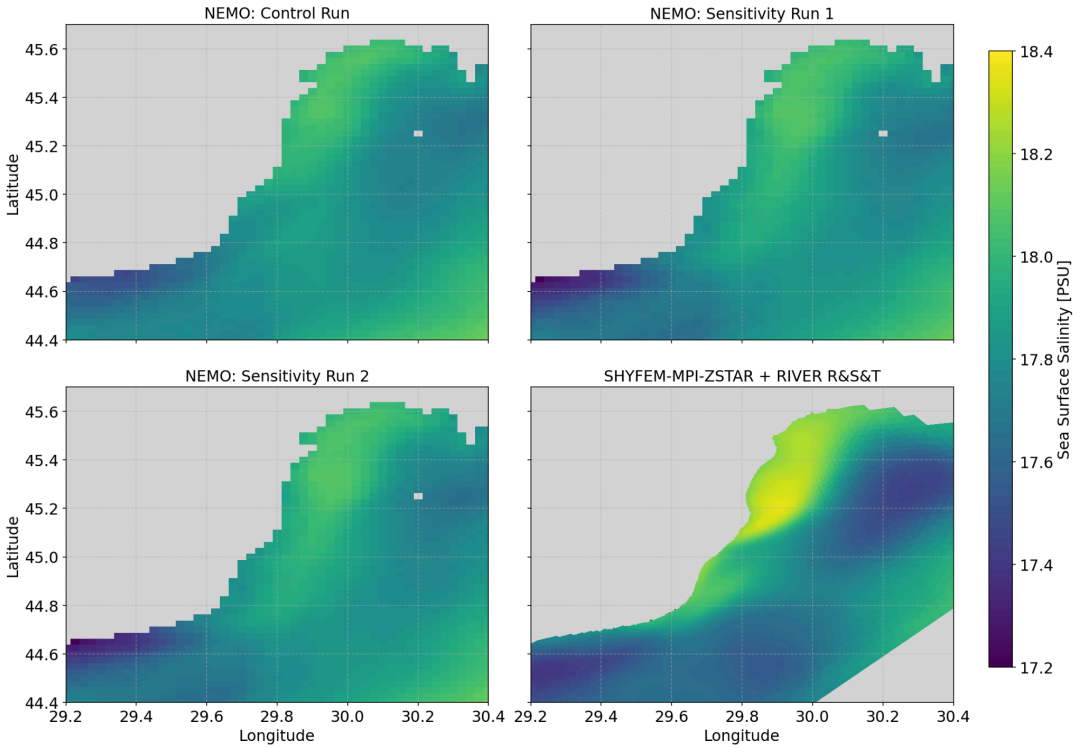


Figure 3.1.4 - Comparison of Sea Salinity at 20m depth simulated by NEMO (Control Run, Sensitivity Run 1, and Sensitivity Run 2) and SHYFEM-MPI-ZSTAR + RIVER R&S&T models during the summer season.

3.2 Po and Ofanto with the Adriatic Sea

Details of the coupled modeling framework are provided in deliverable D4.4; therefore, only updates to the model results are presented here. As the Adriatic regional model is coupled with the riverine inputs from the Po and Ofanto rivers, the spatial improvements of the updated version relative to the reanalysis product are shown in Figures 3.2.1, 3.2.2, 3.2.3, 3.2.4 (Po) and Figures 3.2.5, 3.2.6, 3.2.7, and 3.2.8 (Ofanto). For simplicity, only the winter and summer results are presented in terms of spatial variability, although the annual mean and the other seasonal averages were also evaluated (not shown).

Figures 3.2.4 and 3.2.6 show that sea surface temperatures are consistently warmer during winter across most of the northern Adriatic compared with the reanalysis, except in the vicinity of the Po Delta, where the riverine input produces cooler conditions. In contrast, summer results show generally cooler sea surface temperatures than the reanalysis, with a localized reversal of the anomaly near the river mouths, where the coupled model predicts warmer waters (Figure 3.2.5). These results highlight the importance of using the EE outputs to provide realistic, time-varying river discharge, salinity, and temperature at the river boundaries, rather than relying on the climatological values that are commonly prescribed in regional ocean models.

.

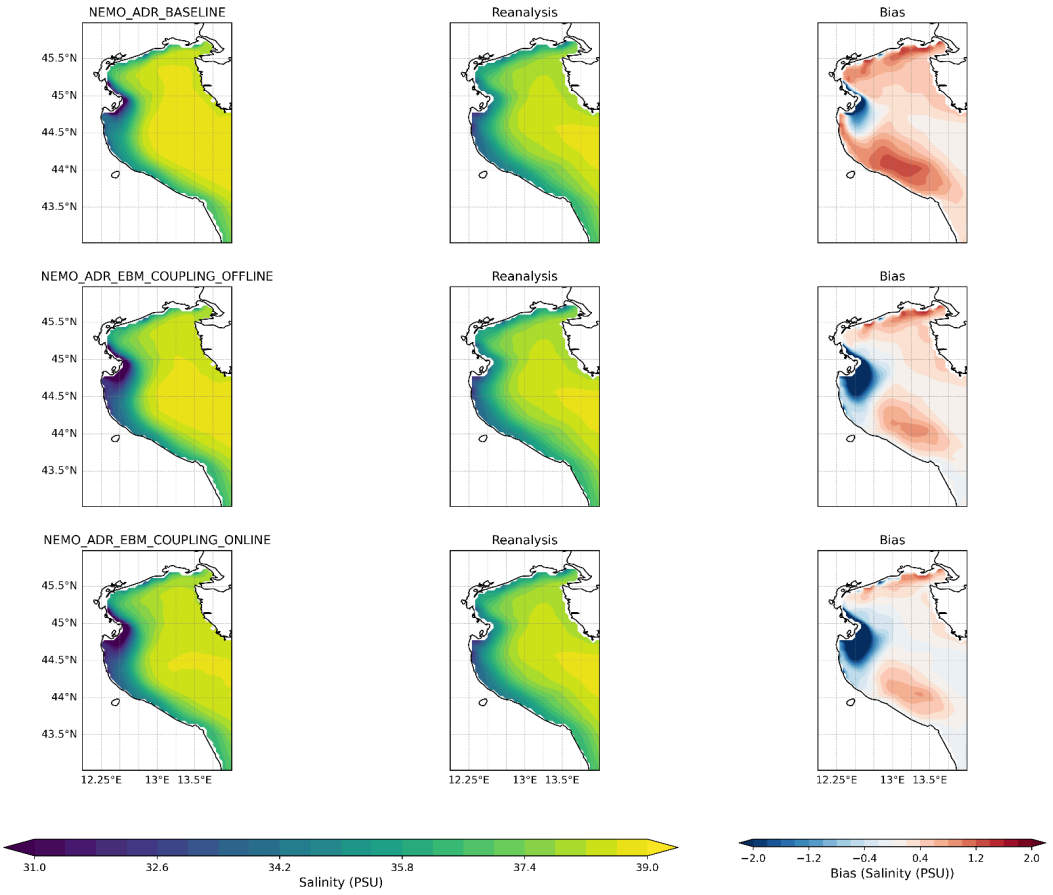


Figure 3.2.1 - Sea surface salinity comparison maps near the Po Delta for winter, between experiments and CMEMS Reanalysis.

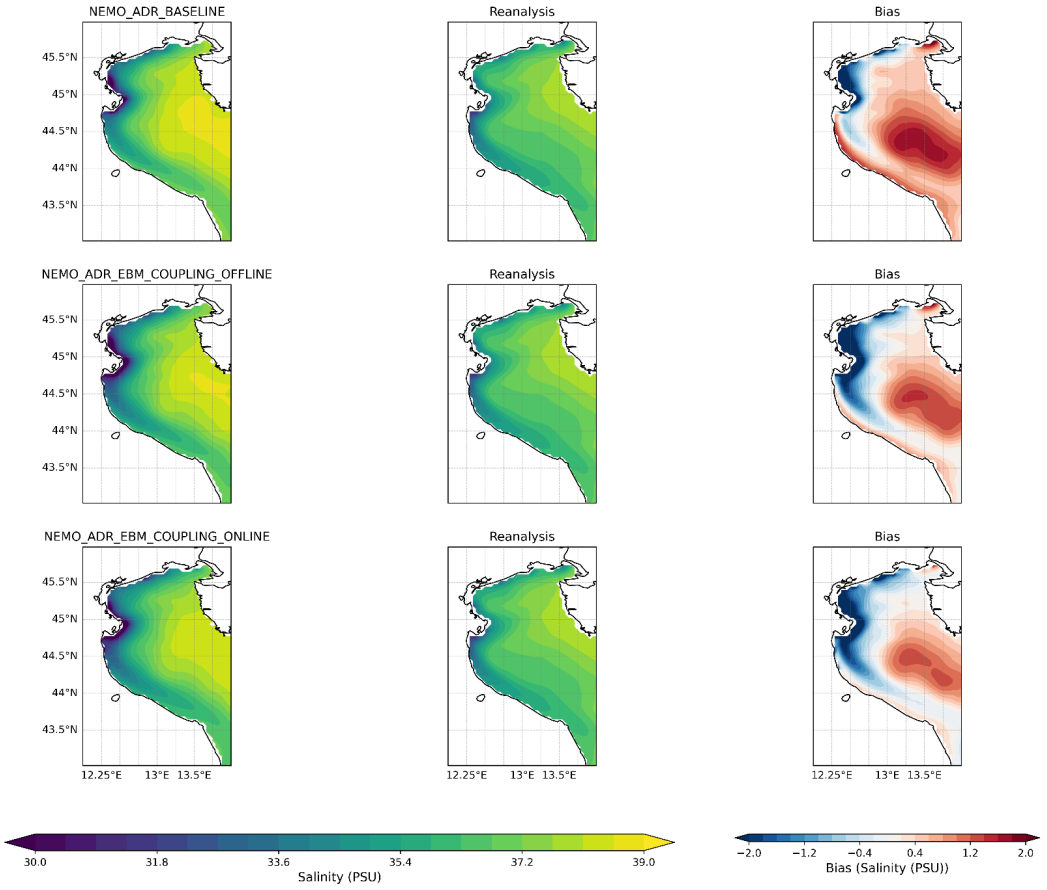


Figure 3.2.2 - Sea surface salinity comparison maps near the Po Delta for summer, between experiments and CMEMS Reanalysis.

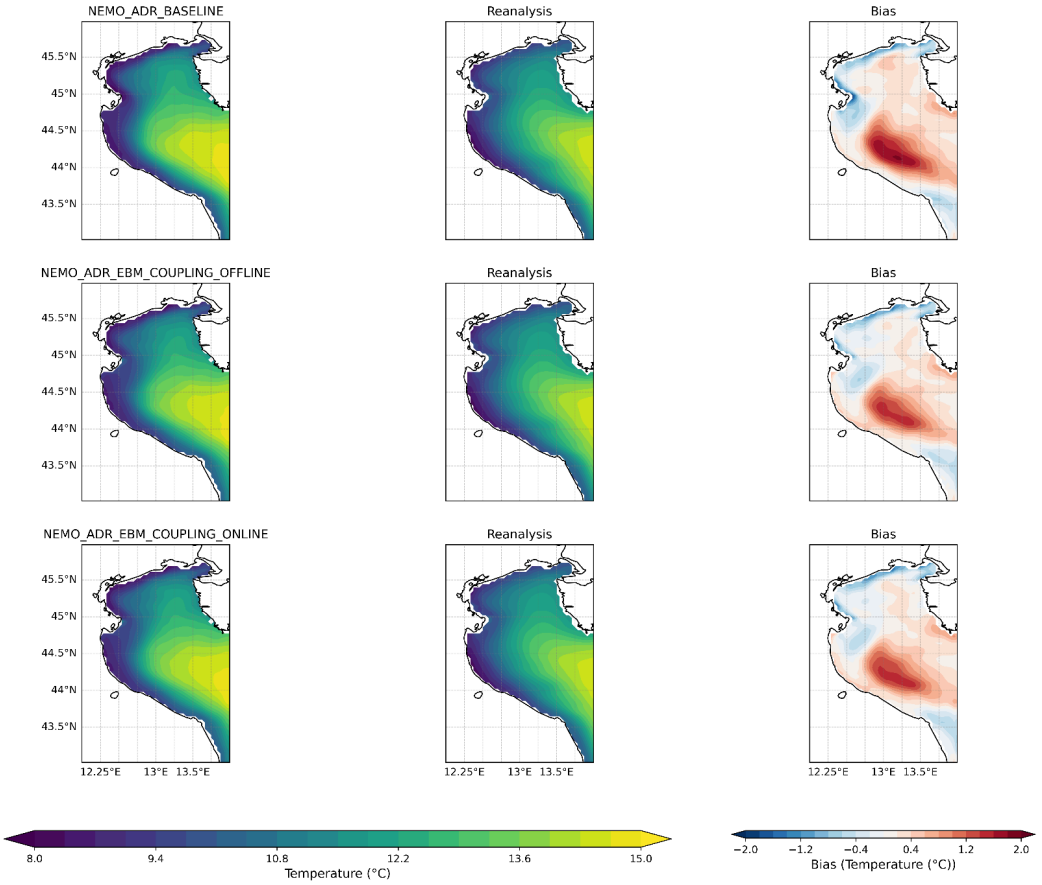


Figure 3.2.3 - Sea surface temperature comparison maps near the Po Delta for winter, between experiments and CMEMS Reanalysis.

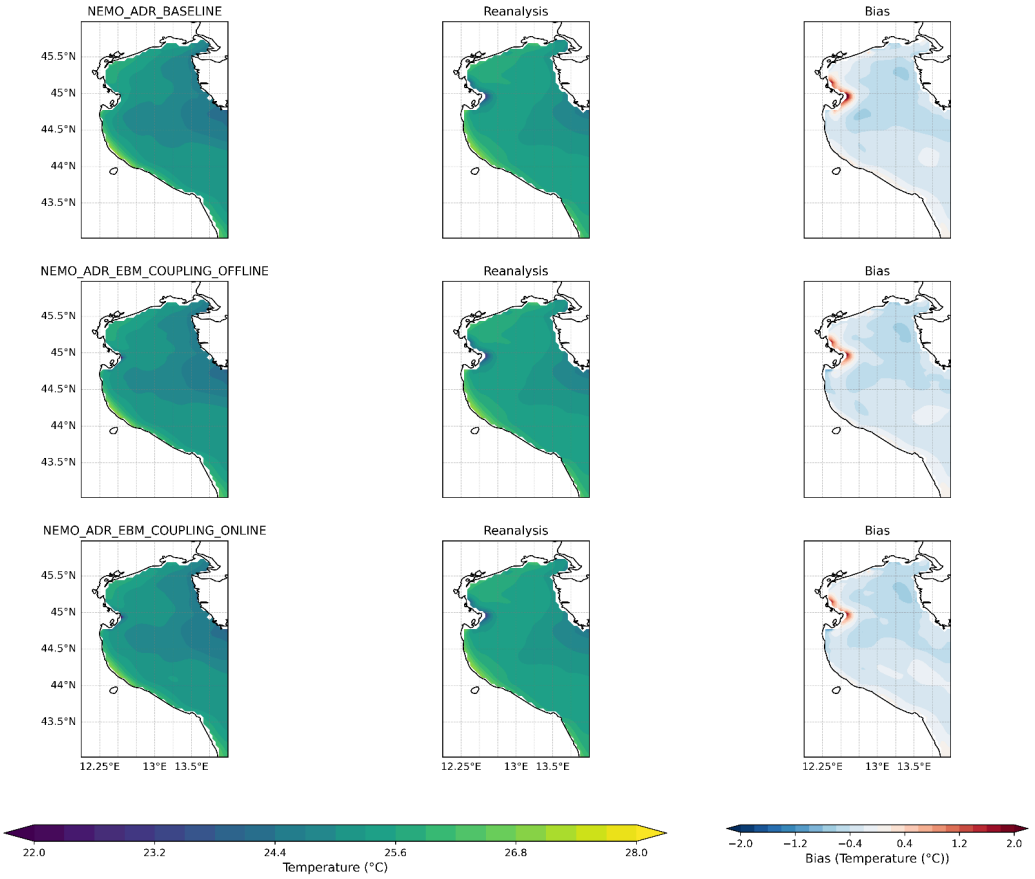


Figure 3.2.4 - Sea surface temperature comparison maps near the Po Delta for summer, between experiments and CMEMS Reanalysis.

As the Ofanto is a relatively small river with a limited influence on the surrounding coastal waters, the impact of the coupled framework between the EE and the regional model is also modest, although still clearly discernible depending on the season. The coupled simulation produces lower surface salinity values in the coastal area adjacent to the river mouth during both summer and winter. In terms of temperature, the coupled model predicts slightly lower sea surface temperatures near the river mouth during winter, whereas only negligible differences are observed during summer.

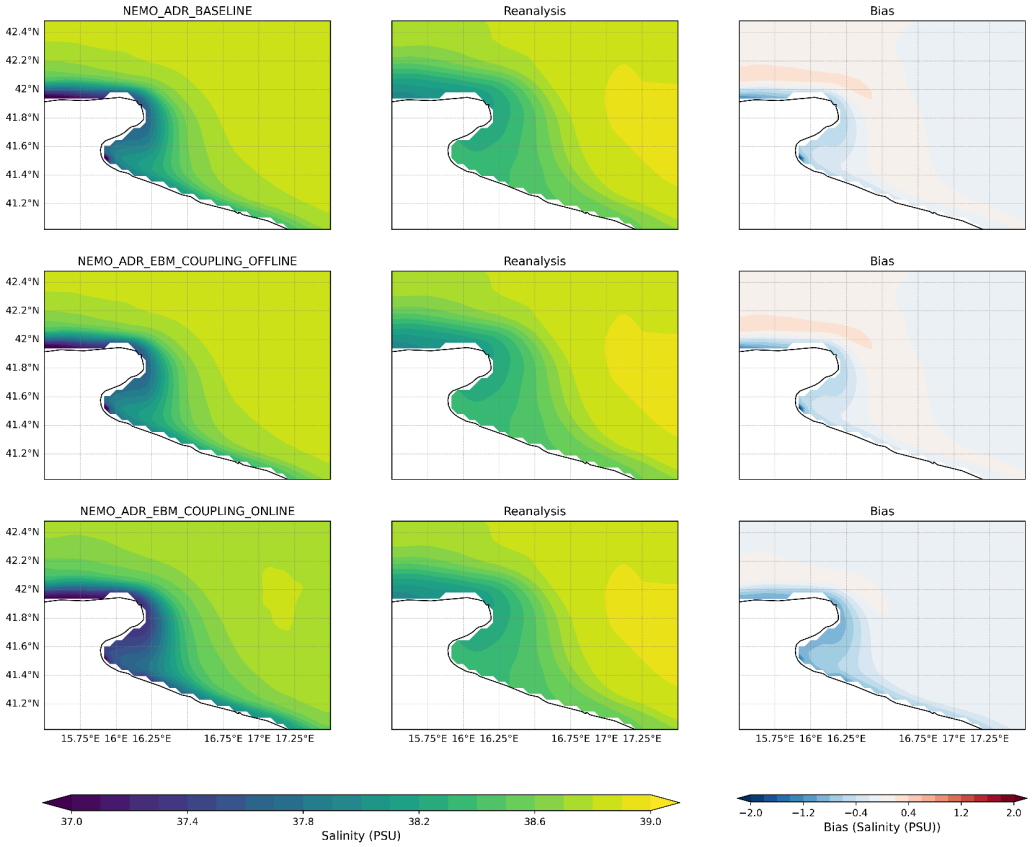


Figure 3.2.5 - Sea surface salinity comparison maps near the Ofanto mouth for winter, between experiments and CMEMS Reanalysis.

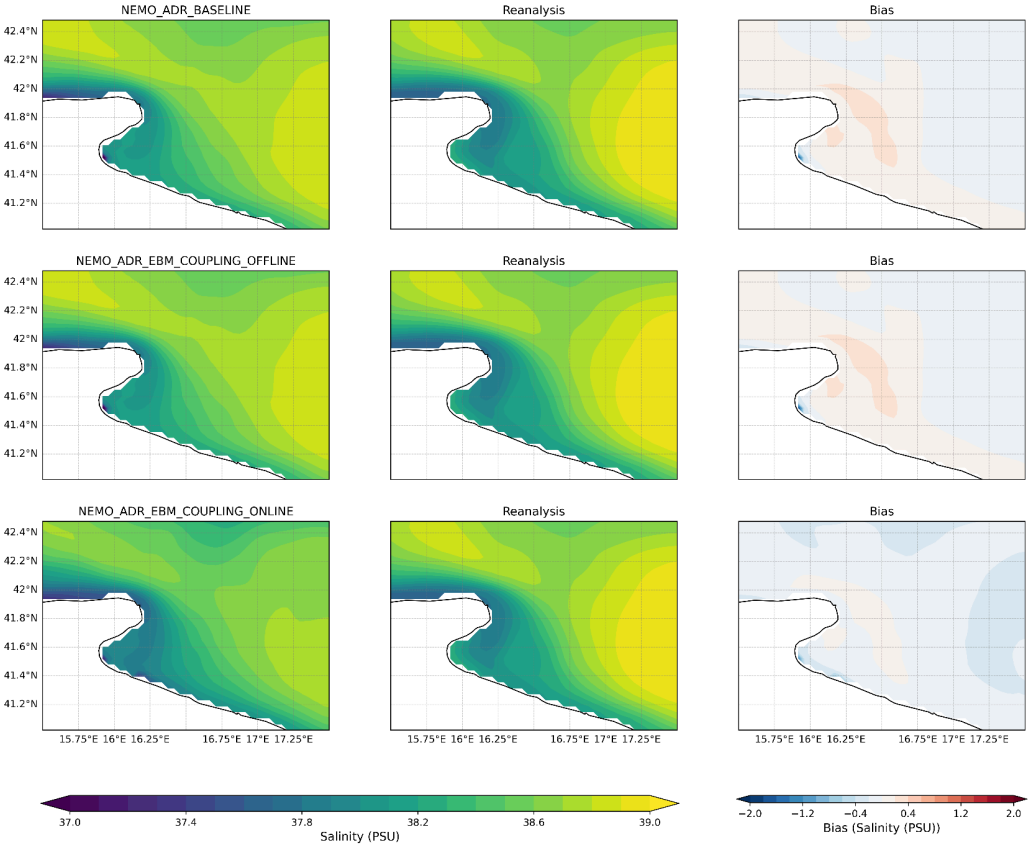


Figure 3.2.6 - Sea surface salinity comparison maps near the Ofanto mouth for summer, between experiments and CMEMS Reanalysis.

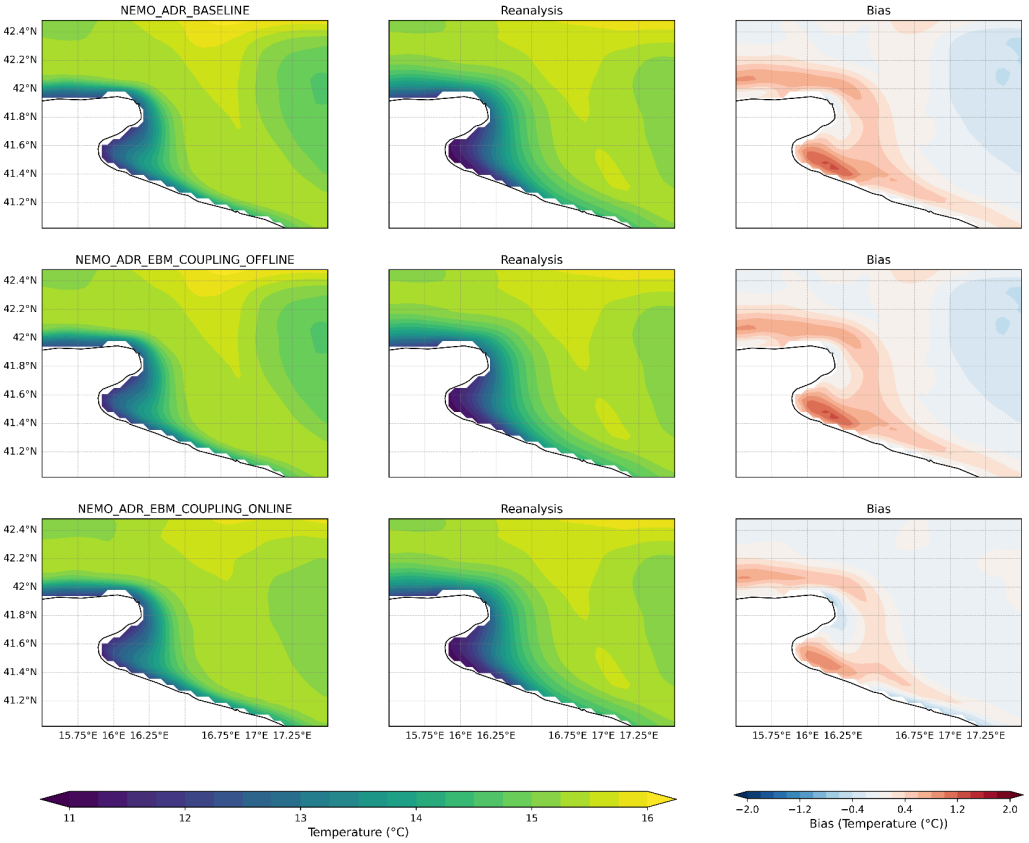


Figure 3.2.7 - Sea surface temperature comparison maps near the Ofanto mouth for winter, between experiments and CMEMS Reanalysis.

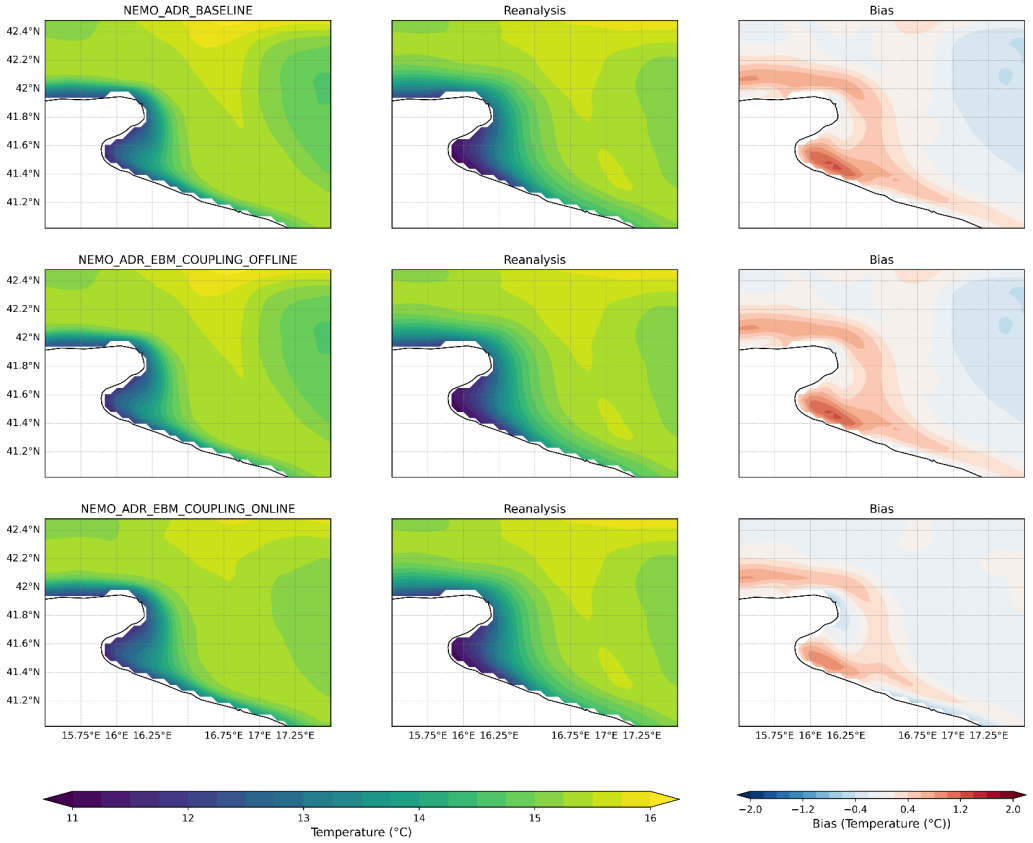


Figure 3.2.8 - Sea surface temperature comparison maps near the Ofanto mouth for summer, between experiments and CMEMS Reanalysis.

Similarly to what was done for the Danube Delta and Black Sea coupled approach, to better assess how the different modeling approaches (standalone NEMO, NEMO offline-coupled with the EE, and NEMO online-coupled with the EE) represent the riverine inputs in comparison with the 3D hyper-resolution LoC model, the figures below show the spatial distribution of salinity and temperature during the season of maximum river discharge, when the influence of the river plume on the coastal zone is greatest. Around the Po Delta (Figure 3.1.9), the superficial freshwater plume is well resolved by the 3D hyper-resolution model, whereas it is substantially underestimated by the standalone NEMO simulation. Coupling NEMO with the EE, either through the online or offline approach, results in a much better representation of the river signature in terms of surface salinity. In both coupled configurations, however, the plume appears more diffuse and spatially smoother than in the hyper-resolution model, as expected given the coarser model resolution. Nevertheless, the coupled simulations reduce the surface salinity by more than 10 PSU near the main Po river mouths compared with the standalone simulation, substantially improving the representation and tracking of

the river plume in the coastal zone. Below the surface, the influence of the riverine input is already greatly reduced. At 5 m depth (Figure 3.1.10), salinity differences decrease from tens of PSU at the surface to only a few PSU, indicating that mixing occurs predominantly within the upper meters of the water column. At this depth, both coupled configurations consistently produce lower salinity around the Po Delta than the standalone NEMO simulation, demonstrating that integrating the EE improves the representation of the riverine plume of the Po Delta influence not only at the surface but also within the water column.

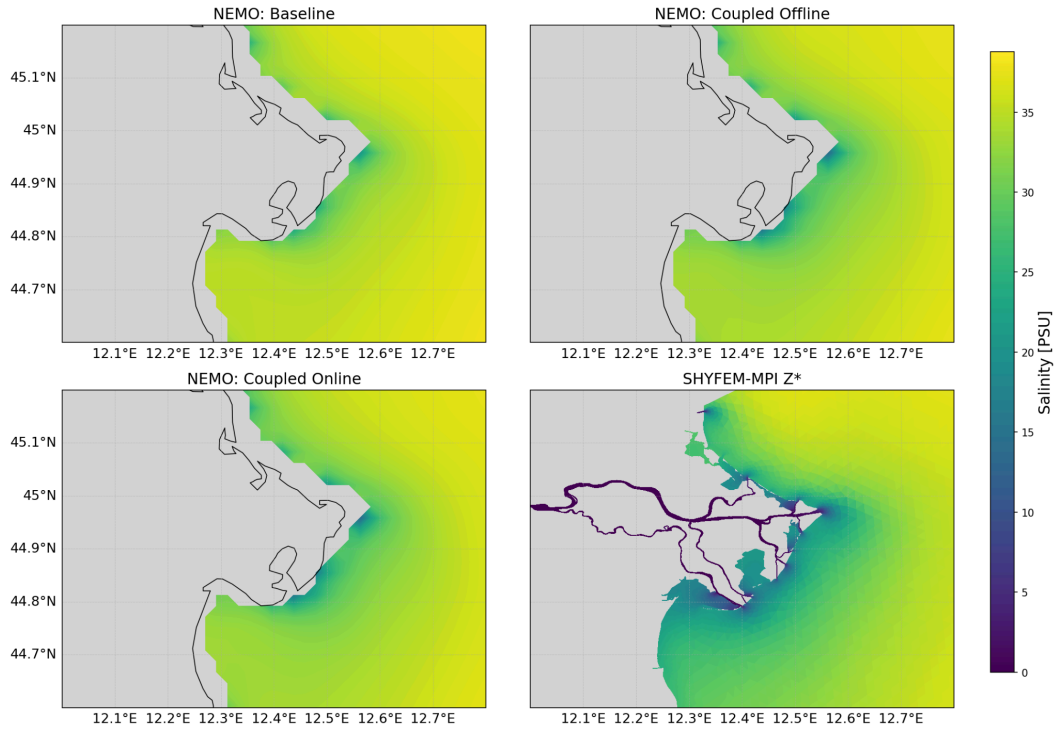


Figure 3.1.9 - Comparison of Sea Surface Salinity (SSS) simulated by NEMO (Base line, coupled offline, and coupled online) and SHYFEM-MPI Z models during the winter season for the area close to the Po Delta.*

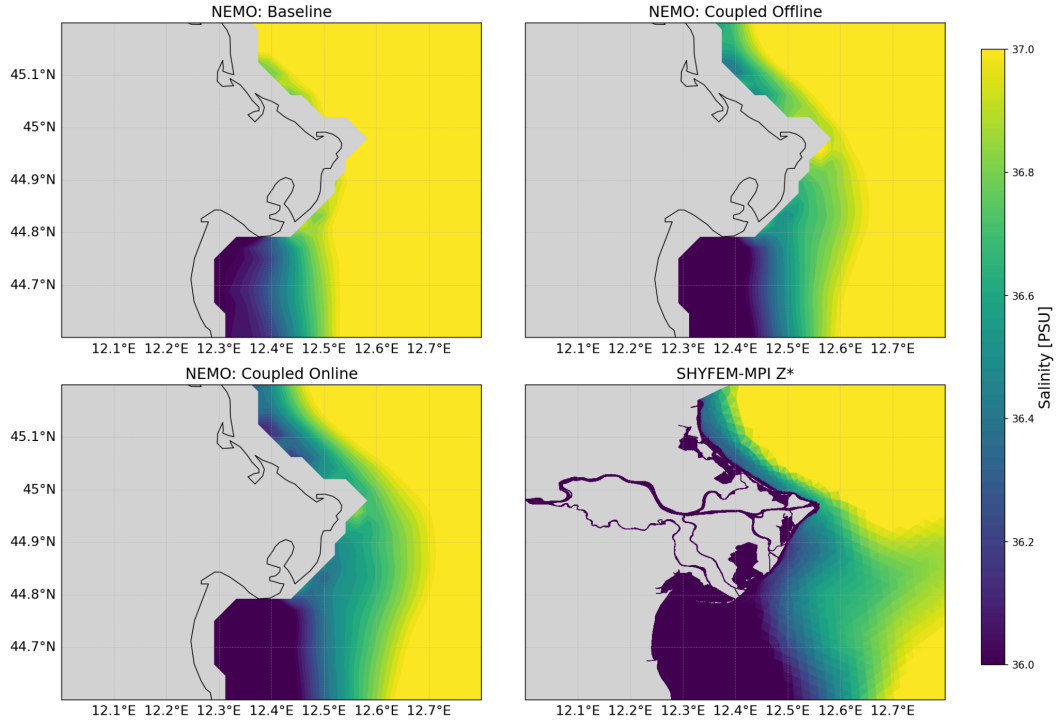


Figure 3.1.10 - Comparison of salinity at 5 m depth simulated by NEMO (Base line, coupled offline, and coupled online) and SHYFEM-MPI Z models during the winter season for the area close to the Po Delta.*

Given the relatively low discharge of the Ofanto River, its influence on the coastal zone is also limited as already mentioned, resulting in smaller differences between the standalone regional model and the coupled configurations. This is evident in the sea surface salinity maps shown in Figure 3.1.11, where a well-defined river plume is resolved only by the 3D hyper-resolution model (bottom right panel). Owing to its coarse resolution, the regional model is unable to adequately represent such a small-scale river plume, even in the season of higher river runoff values (winter).

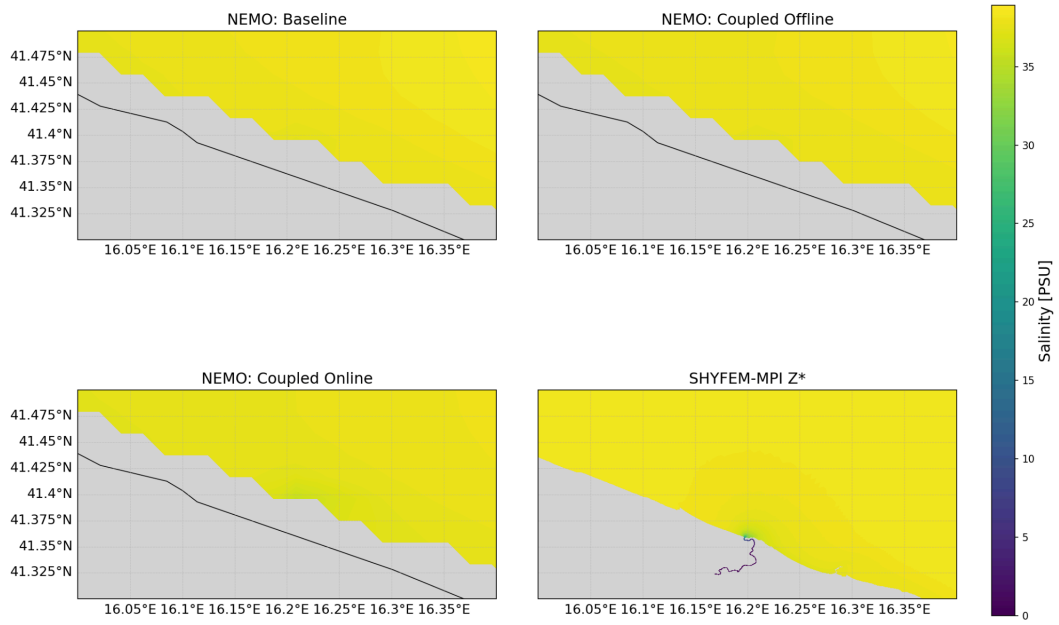


Figure 3.1.11 - Comparison of Sea Surface Salinity (SSS) simulated by NEMO (Base line, coupled offline, and coupled online) and SHYFEM-MPI Z models during the winter season for the area close to the Ofanto mouth.*

Despite the relatively short validation period (1 October to 31 December 2019), from figures 3.1.11 and 3.1.12 it is possible to see that the different NEMO configurations successfully capture the variability in surface salinity associated with the river plume (Figure 3.1.11), whereas the reanalysis fails to reproduce the salinity fluctuations driven by changes in river discharge. The fact that the standalone NEMO simulation (the blue line in Figure 3.1.11) also reproduces the main decreases in salinity indicates that the increased model resolution alone plays an important role in resolving the river plume. Likewise, the offline-coupled configuration (the red line in Figure 3.1.11) successfully captures the overall evolution of surface salinity. However, only the online-coupled configuration provides the closest agreement with observations, particularly during the most pronounced freshwater events.

At a coastal station located outside the area directly influenced by the Po Delta, the pronounced salinity drops observed at the beginning and end of November 2019 are also evident. These events are not captured by the reanalysis, whereas all NEMO simulations reproduce them. However, only the online-coupled configuration is able to reduce salinity below 27 PSU and 23 PSU during the first and second events, respectively, providing the closest agreement with observations. The offline-coupled approach, instead, produces results very close to the standalone NEMO. This

demonstrates not only the added value of integrating the EE with mesoscale ocean models, but also that its benefits are further enhanced through online coupling. By enabling a two-way exchange of information between the EE and the regional ocean model, the online framework provides more realistic and time-varying riverine conditions, leading to a more accurate representation of river inputs on coastal zones, which are crucial for the circulation dynamics of the Adriatic Sea.



Figure 3.1.10 - Position of the two coastal buoys used to evaluate the model performance in representing salinity variability.

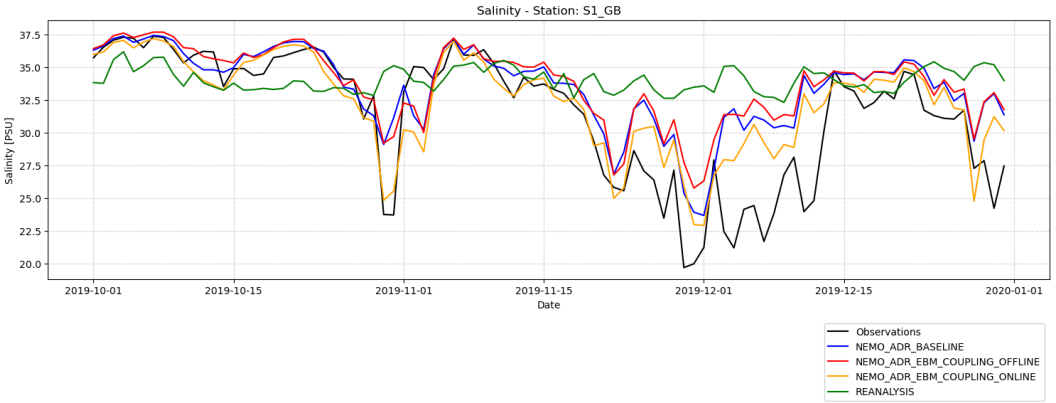


Figure 3.1.11 - Comparison of the different modeling approaches, the reanalysis, and the observations at station S1, located offshore of the Po Delta.

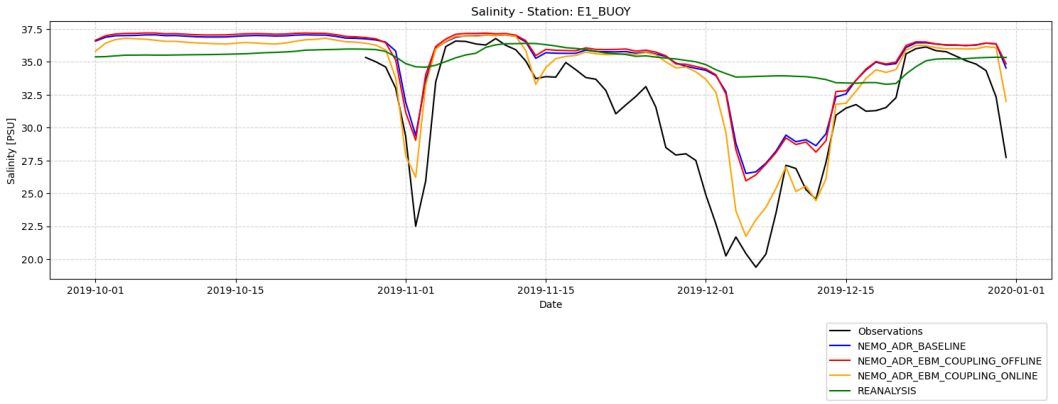


Figure 3.1.12 - Comparison of the different modeling approaches, the reanalysis, and the observations at station E1, located offshore of the Po Delta.

3.3 Tagus and Sado Estuaries and the Portuguese Coast

This section describes the coupling of the EE with the Portuguese Circulation Operational Modelling System (PCOMS), and its comparison with the standard operational implementation.

The PCOMS system is a 3D full baroclinic hydrodynamic and biogeochemical regional ocean operational model application that uses MOHID Water as its numerical core. It is composed of two nested domains: WestIberia (2D) and Portugal (3D) covering the Iberian Atlantic coast and its contiguous ocean. Both domains use a constant horizontal spatial resolution of 0.06°, resulting in a 6.7 × 5.2 km domain. The Portugal domain is located at the centre of the WestIberia grid. Vertically, it uses a hybrid discretisation with a near-surface, variable-thickness sigma layer with 12 levels, increasing from 1 m at the surface to 19.94 m in depth, above a layer with 63-z-levels increasing in thickness towards the bottom.

Tides are forced with FES2014 harmonic components along the WestIberia domain boundary. The Portugal domain receives tides from the WestIberia domain, and uses the Copernicus Global Ocean 1/12° Physics Analysis and Forecast updated daily product (hereafter referred as CMEMS-Global) as initial and boundary conditions for water levels, currents, temperature, and salinity. At the atmospheric boundary, the Portugal domain is forced by results from the meteorological model AROME operated by the Portuguese Institute for the Sea and Atmosphere (IPMA), and GFS from

NOAA. The EE from the main Portuguese rivers provide fluxes, temperature, salinity, and velocity time series in the continental boundary condition (Figure 3.3.1).

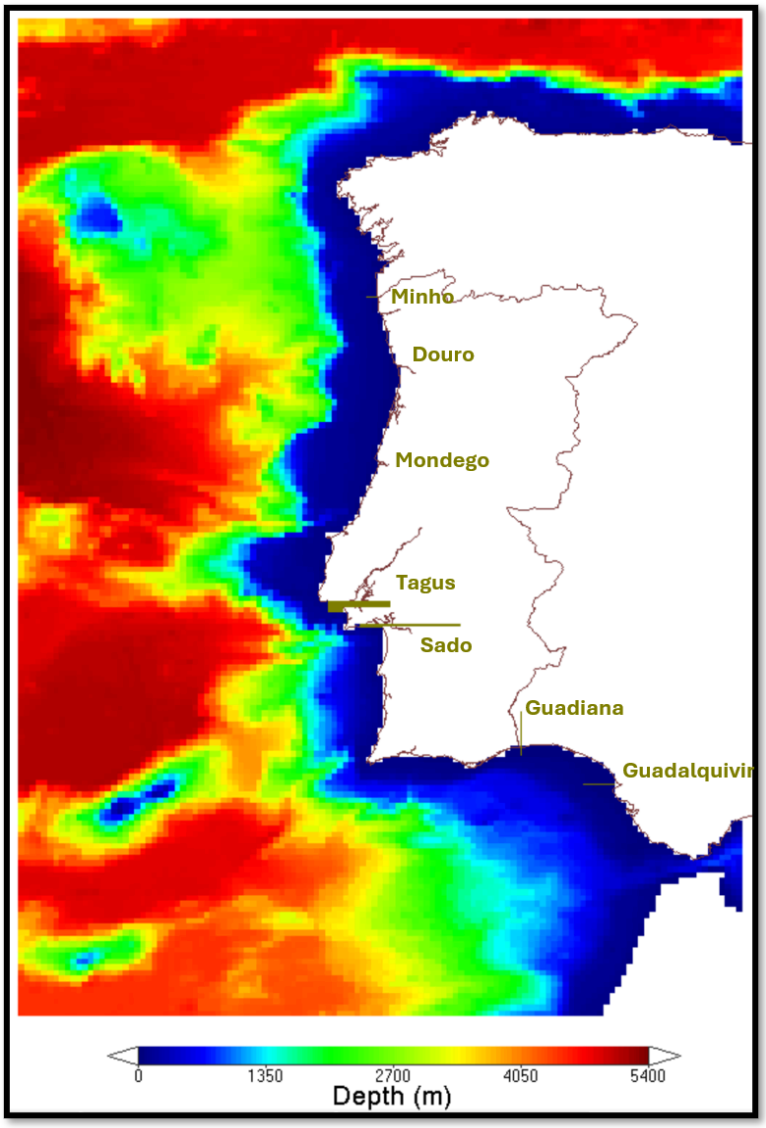


Figure 3.3.1 - Domain and bathymetry of the Portuguese Coastal Operational Modelling System (PCOMS) and the location of the main river estuaries emulators considered, including the Minho, Douro, Mondego, Tagus, Sado, Guadiana and Guadalquivir rivers.

Figure 3.3.2 compares the sea surface salinity simulated by PCOMS both without and with river discharge forcing provided through the EE interface. In the absence of river inputs, the coastal domain is characterised by relatively homogeneous salinity values, reflecting predominantly oceanic conditions with limited spatial variability. The inclusion of river discharge forcing substantially

modifies the coastal salinity distribution, generating distinct low-salinity plumes at the mouths of the main Portuguese rivers. These freshwater plumes are subsequently advected along the continental shelf by coastal circulation, increasing the spatial heterogeneity of the salinity field and enhancing the representation of land-ocean interactions. The largest impacts are observed in the vicinity of the Tagus and Douro estuaries, which receive freshwater from two of the largest river basins draining into Portuguese territory, and represent major contributors to the total river discharge along the Portuguese coast. During periods of high river discharge, their freshwater inputs significantly alter the nearshore salinity structure and enhance the development of coastal freshwater plumes.

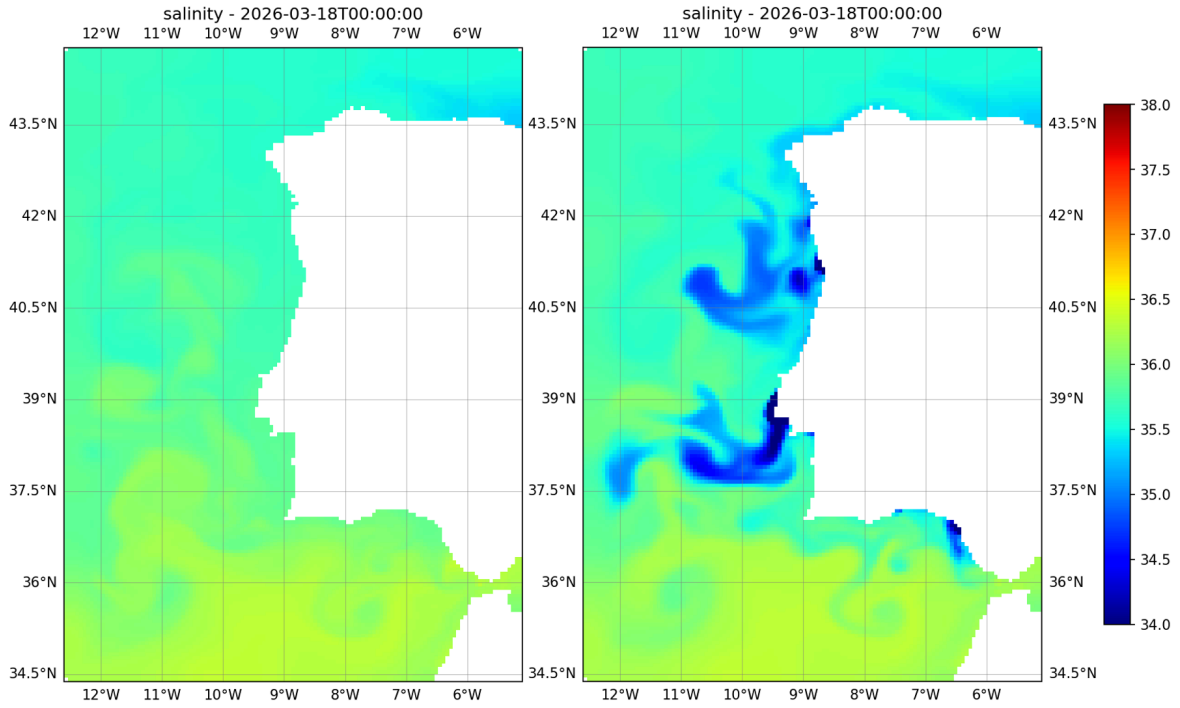


Figure 3.3.2 - Sea surface salinity from PCOMS. The left panel shows the simulation without river discharges, while the right panel includes the contribution of the main river inputs. A clear decrease in coastal salinity is observed in the river-influenced scenario, under an extreme river flow event, highlighting the impact of freshwater input on the coastal salinity structure.

Figure 3.3.3 compares the sea surface salinity simulated by PCOMS with the corresponding Copernicus satellite product for 18 March 2026. Overall, the regional model reproduces the large-scale salinity distribution over the western Iberian shelf reasonably well. Both datasets show a predominantly homogeneous offshore salinity field, with values generally ranging between 35.0 and 36.0 PSU, while lower salinity waters are observed along the continental shelf. In both maps the

presence of elongated filaments and coastal tongues of relatively fresh water extending offshore from the Portuguese coast are visible. These structures are particularly evident off the western and southwestern coasts, indicating the influence of river discharge and coastal circulation processes. The model captures the general position and orientation of these low-salinity features, suggesting that the dominant mesoscale circulation patterns are well represented. However, some differences are also apparent. The model exhibits sharper and more coherent filament structures, with stronger salinity gradients near the coast. In contrast, the satellite data produces a smoother salinity distribution, with broader transition zones between low- and high-salinity waters. This smoothing may result from differences in horizontal resolution (lower spatial resolution of the satellite product), or the treatment of mixing processes within the model. Additional discrepancies are observed in the northern part of the domain, particularly in the Bay of Biscay, where the model simulates lower salinity than the satellite product. This mismatch is likely related to the specification of the open boundary conditions and the lack of river discharge forcing along the northern boundary of the model domain, limiting the model's ability to accurately reproduce the freshwater distribution in this region.

Despite these local differences, the comparison demonstrates that the regional model successfully reproduces the main spatial patterns of sea surface salinity over the Portuguese continental shelf. The overall agreement indicates that the model provides a realistic representation of the large-scale hydrographic conditions, while also highlighting the importance of including realistic river discharge forcing to accurately reproduce coastal and shelf circulation and salinity distribution.

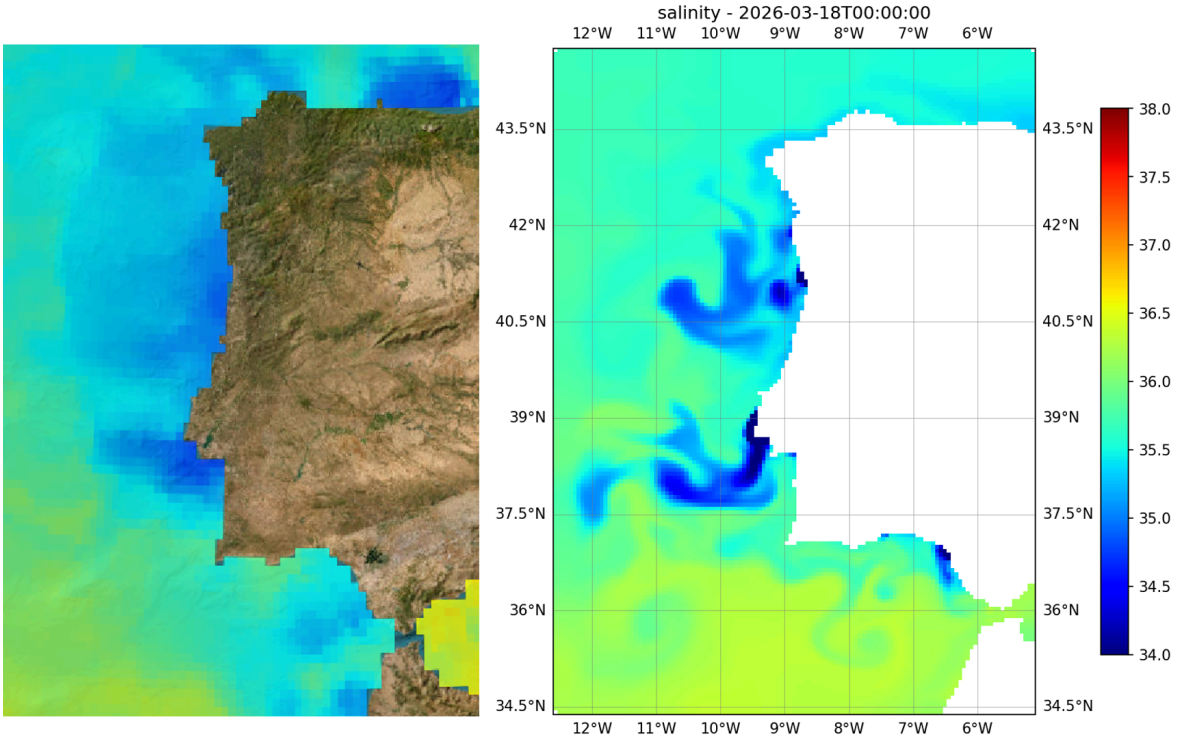


Figure 3.3.3 - Left: Satellite-derived Near Real-Time (NRT) daily sea surface salinity data at approximately 12.5 km spatial resolution, L4, Multi-sensor (SMAP, SMOS) from CMEMS. Right: Sea surface salinity from PCOMS with river forcing from EE. Both maps are from 18th March 2026.

3.4 Dutch Continental Shelf

As part of this task, Deltares has integrated E-HYPE 4.3.2 river discharge outputs into the Dutch Continental Shelf Model (DCSM), for both the hydrological and biogeochemical variables. The following section highlights the differences in biogeochemical model outcomes between the previous model configuration and the new setup incorporating E-HYPE discharges. The section first outlines the key differences between the former and updated model setup. It then introduces the model performance assessment framework and evaluates the resulting differences in model outputs. The section ends with additional benefits of using E-HYPE and future research opportunities.

3.4.1 Model Setup Differences

In earlier DCSM configurations (Vilmin et al, 2026), river discharge inputs were derived from the ICG-EMO-RID V0 Version 4 (September 2024) dataset originally developed to support the OSPAR Eutrophication Assessments (van Leeuwen, 2024). Only discharge points classified as rivers were

included, yielding 319 discharge locations based on observational data collected between 1990 and 2022. The dataset provides discharge and daily loads for NH_4, NO_3, Total N, PO_4, Total P, SPM, Si, Fe, NO_2, TALK, DIC, DOC, TOC, and POC. Missing data were filled using linear interpolation for gaps of ≤ 50 days, and climatological means for gaps > 50 days. The frequency of such gaps, and therefore the reliability of each time series, varies by country, depending on national data availability.

In the updated DCSM discharge configuration, all discharge locations (both rivers and direct discharges) from the E-HYPE 4.3.2 dataset within the model domain have been implemented. The dataset delivers freshwater discharge and concentrations of inorganic nitrogen, organic nitrogen, total nitrogen, soluble (reactive) phosphorus, particulate phosphorus, total phosphorus, and total suspended solids from 2000 to 2024.

As a result, the updated configuration now includes 1,526 discharge locations from E-HYPE 4.3.2 (see Figure 3.4.1). This model setup was run for one year, 2015.

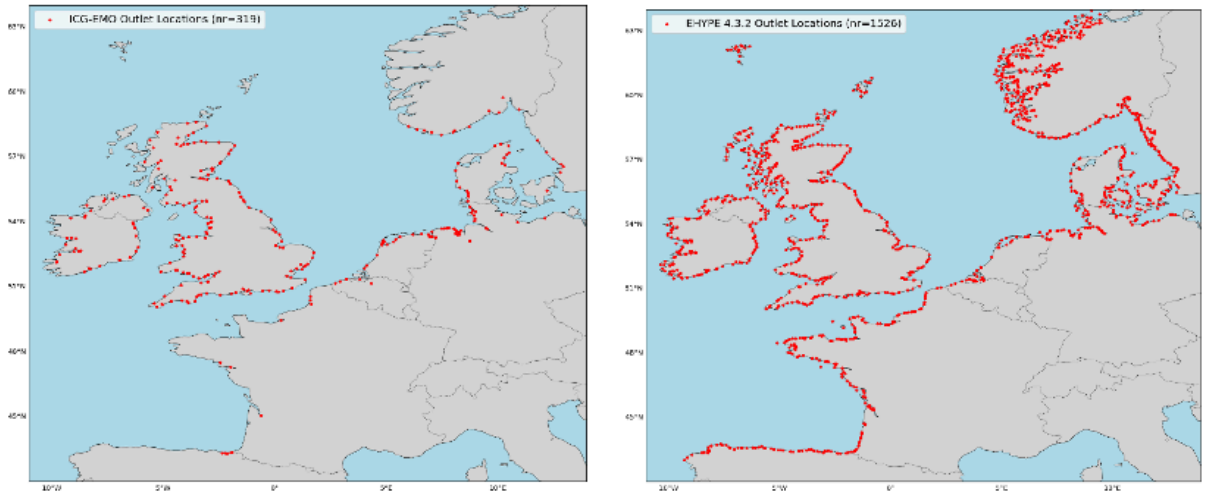


Figure 3.4.1 - River or Direct discharge locations in previous model setup (left) and River or Direct discharge locations in new model setup (right), with E-HYPE 4.3.2.

3.4.2 Measurement Observations

For the model performance assessment, a subset of the database used for the assessment of all versions of the Dutch MSCS, the North and Wadden Sea Data Management database, was used (Stolte, 2023). This database is maintained by Deltares and includes various data sources from the main data owners of North Sea and Wadden Sea data at >3.500.000 locations. The database covers 31 parameters (e.g. chlorophyll, nutrients, particulate organics, primary production, pH, alkalinity,

temperature, salinity, O2). Data is sourced from EMODnet, ICES, SOCAT, and complemented by national databases: PML, NIOZ, VLIZ, Schlesswig-Holstein, RBINS, Danish MSFD database, CEFAS, IFREMER, IMR, MSS, SMHI, NLWKN, Rijkswaterstaat, Macovei, HZG. The full database covers the period 1893-2024.

For the following model performance assessment, a 2015 subset for chlorophyll-a, NO3, and PO4 at the water surface was produced. The available measurement data were then matched to the observation-station locations specified in the DCSM, which record daily model results at those locations. The matched observation stations containing more than four measurements in 2015 are shown in Figure 3.4.2.

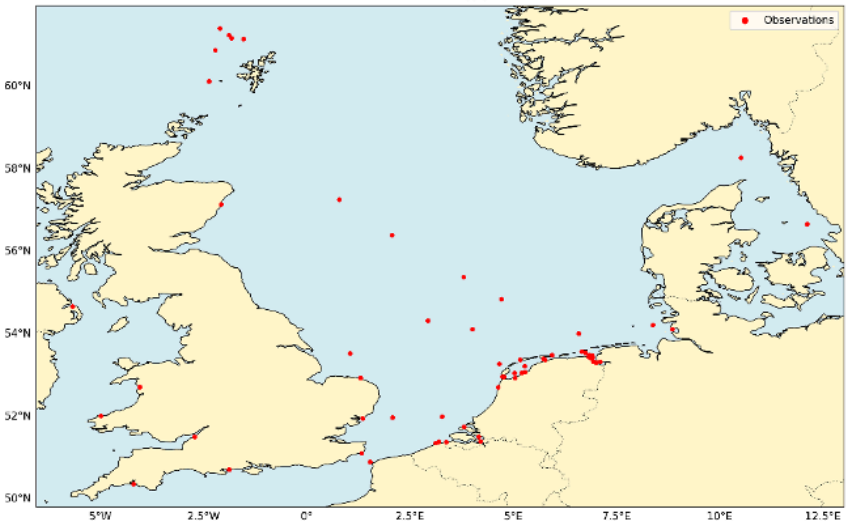


Figure 3.4.2 - Matched NDWM measurement locations and DCSM observation stations with more than 4 measurements for Chlorophyll-a, NO3 and PO4 for 2015.

3.4.3 Model Performance Evaluation

Model performance for 2015 was evaluated using RMSE and the coefficient of determination (R^2) across all matched observation stations. When aggregated over all stations, nitrate (NO_3), phosphate (PO_4), and chlorophyll-a show higher annual error metrics in the configuration using E-HYPE 4.3.2 compared to the previous discharge setup. This indicates a general degradation in overall model skill for these parameters when switching to E-HYPE at the basin-wide scale (Figure 3.4.3).

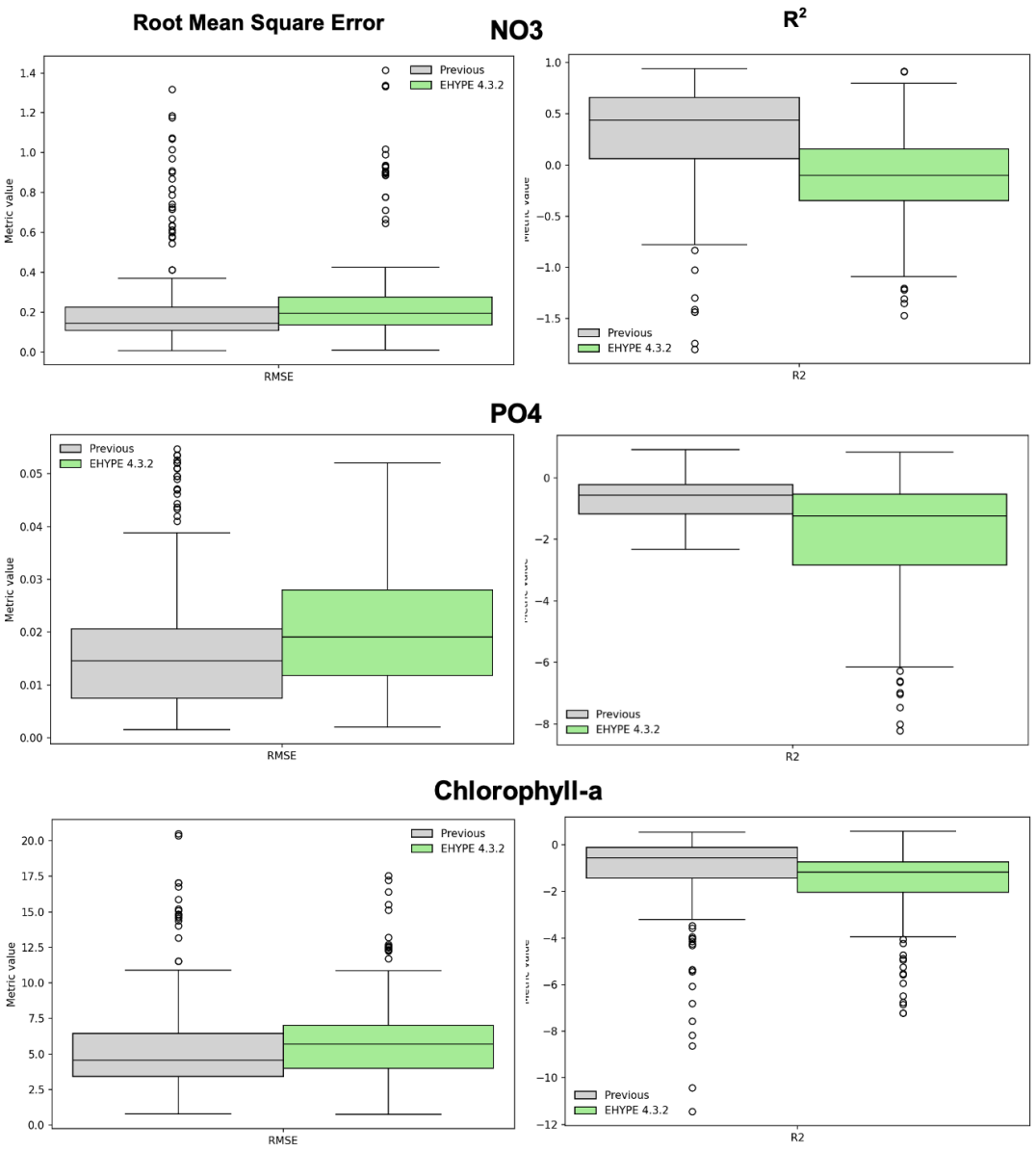


Figure 3.4.3 - Annual station-level error metrics. RMSE (left) for NO_3 (top), PO_4 (middle), and chlorophyll-a (bottom) and R^2 (right). Previous model setup is shown in grey and EHYPE 4.3.2 in green; boxes show medians and interquartile ranges.

To further investigate the spatial nature of these differences, observation stations were separated into those located within the Dutch Exclusive Economic Zone (EEZ) and those outside it (Figure 3.4.4). This distinction reveals that the increase in error metrics is primarily associated with stations within the Dutch EEZ. At the non-Dutch stations, we find that the RMSE and R2 between the model setup and measurements are similar (and sometimes better) between both model setups. For NO3, the

mean RMSE of both model setups is nearly identical, whereas the coefficient of determination has fewer outliers when using E-HYPE 4.3.2. For PO4, we also find that RMSE of both model setups is very similar, as well as the coefficient of determination which has slightly fewer outliers when using E-HYPE 4.3.2. In regards to Chlorophyll-a, we find that both the RMSE and R2 are slightly worse, no matter at which observation stations.

Overall, these results indicate that replacing the previous river discharge dataset with E-HYPE 4.3.2 leads to reduced model performance within the Dutch EEZ, while having a neutral to slightly positive effect on model accuracy outside this region. From a performance perspective, this suggests that E-HYPE 4.3.2 is currently more suitable for use in areas beyond the Dutch EEZ, rather than the core region of interest of the Dutch MSCS.

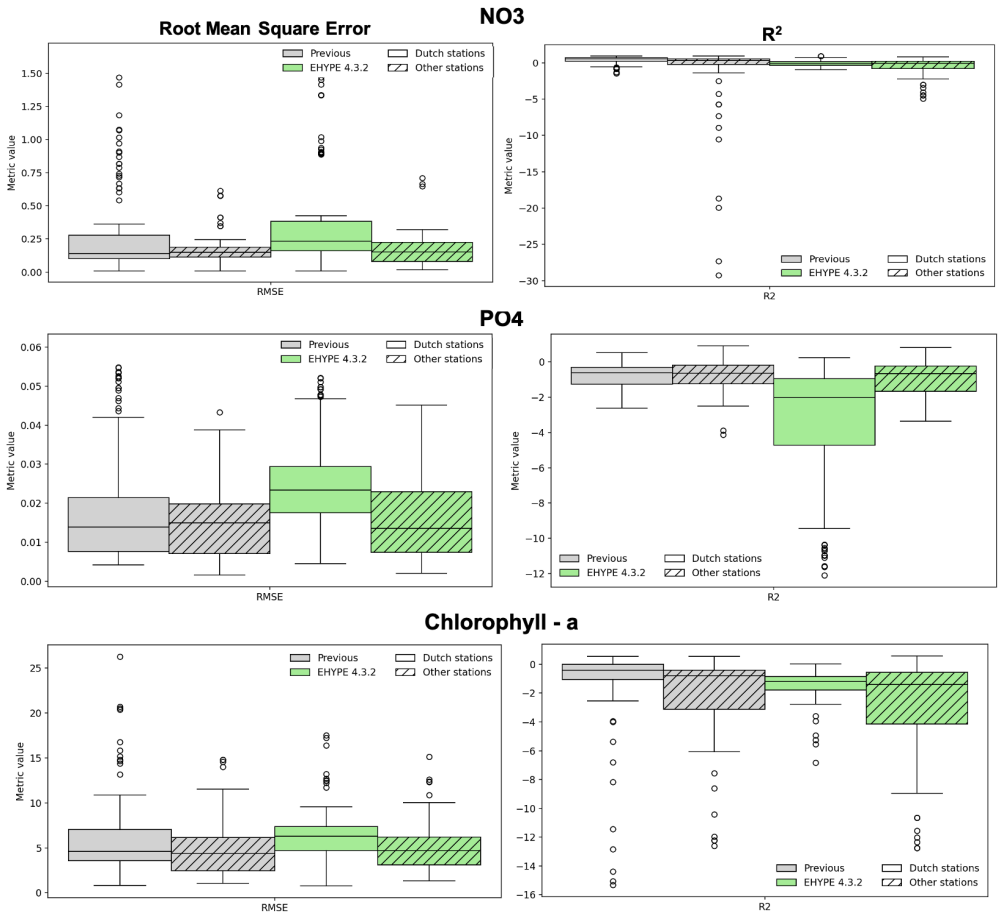


Figure 3.4.4 - Annual station-level error metrics. RMSE (left) for NO_3 (top), PO_4 (middle), and chlorophyll-a (bottom) and R^2 (right). Previous setup is shown in grey, EHYPE 4.3.2 in green; Dutch stations are unhatched and other stations are hatched. Boxes show medians and interquartile ranges

3.4.4 Other Benefits of E-HYPE

Although the model performance does not benefit greatly from the use of E-HYPE compared to previously used river databases, the use of hydrological model data instead of gap-filled observations does have its benefits, which, depending on the use-case, might outweigh the differences in model performance.

First, using modelled hydrological results allows for the calculations of future and historical scenarios, which is not possible with a gap-filled observational dataset. Therefore, E-HYPE has the potential to be used in climate change, historical, and future long-term scenarios for coastal models, whilst gap-filled datasets cannot be used for scenarios beyond 2024.

Second, the common processing between all discharge locations in a hydrological model produces a more consistent temporal result. Discharge inputs are then not reliant on missing data and different degrees of necessary gap-filling to produce temporally consistent results. Similarly, an error in data delivery of observations (such as different units than requested) does not propagate into the coastal model results, which does happen in observation-reliant datasets.

Additionally, another large benefit of using E-HYPE comes into play when looking beyond a single MSCS setup and performance. The pan-European reach of E-HYPE crosses many local and regional MSCS. The use of the same discharge inputs in all of these coastal modelling systems allows for easier and more consistent comparisons between models of different users and communities. Using a harmonised discharge dataset creates an opportunity for inter-model and inter-MSCS comparisons.

3.4.5 Future Recommendations

To make the use of E-HYPE in coastal models easier, there are a couple of recommendations:

- Deliver the E-HYPE results with a clear indicator if the modelled discharge belongs to a river outlet or direct discharge. The current delivery merges multiple discharge types, which makes analysing E-HYPE output and comparison with other coastal river datasets a cumbersome process that requires manual river matching and identification. Currently, this limits large scale input analysis. Distinguishing between the different discharge types in the E-HYPE output could also help in coastal model implementation, as it makes it easier to

decide which discharges are essential to include and contribute most in a specific coastal model setup.

- Also include temperature in E-HYPE. In the latest Zenodo release, the user is forced to deduce temperature from other river or model sources and combine inputs into their coastal model. If E-HYPE could be expanded to also include temperature, it would be an additional advantage.

3.5 Northwestern Black Sea Coastal System

The LoC for the Northwestern Black Sea was reproduced with the GCOAST-BS setup using results from the E-HYPE model (MS4.1; D5.2). The contribution of the small rivers was included in GCOAST-BS and an assessment of the results was presented in section 2.4 from the report D5.3. Here, the capacity of the GCOAST-BS to represent the influence of the far field of the Danube's plume over the Northwestern Black Sea is demonstrated through comparison with satellite images. Sea surface salinity (SSS) and sea surface temperature (SST) fields from the SCHISM model are used as tracers of the riverine input and compared with SST from the Copernicus Marine product SST_BS_SST_L4_REP_OBSERVATIONS_010_022, and suspended particulate matter (SPM) from the CMEMS product OBS-OC_GLO_BGC-TRANSP_MY_L3-MULTI-4KM_P1D. Figure 2.7.1 shows the comparison between GCOAST-BS and satellite for SST for the date 2021.11.22. During this period, a strong SST gradient is present along the continental shelf, and the isotherm of 12°C from GCOAST experiments shows a good agreement with the satellite field. Comparing the results with SCHISM experiments, differences of around 2.00°C occur in the domain. Comparing both experiments, contributions of the freshwater input from the outlets give rise to differences of about 0.25°C.

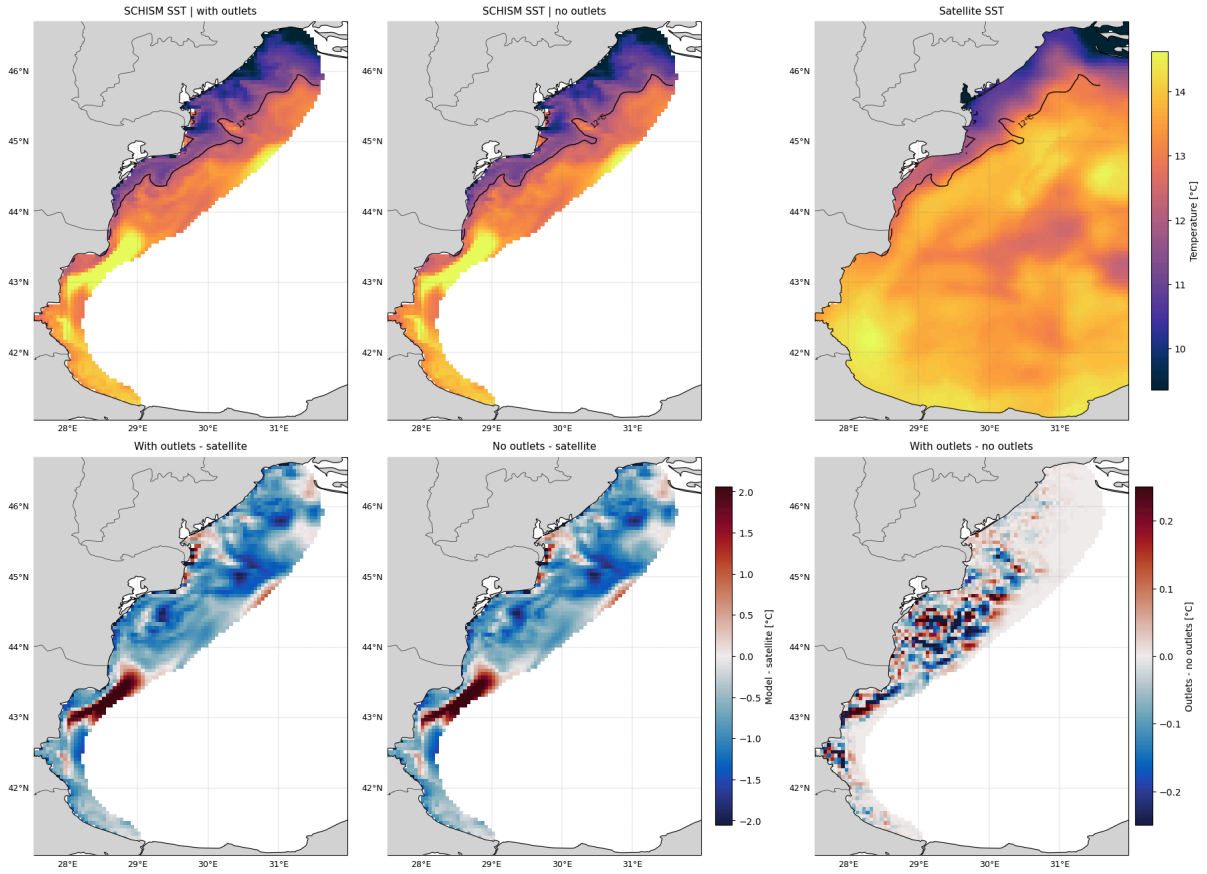


Figure 2.7.1 - Comparison between GCOAST-BS experiments and satellites for the SST fields for 2021.11.22. The upper panel shows the SST fields with the isotherm of 12 °C, highlighting the sharp gradient at the north sector of the domain. Lower panels show the difference between model results and satellite fields in the first two maps, while the third map shows the difference between both results.

Figure 2.7.2 shows the influence of the Danube's plumes using salinity as tracers in the SSS fields. A comparison is made with the satellite field for SPM because SSS observations have a much coarser resolution to be comparable with GCOAST results. The SPM contours are shown over the SCHISM SSS fields, while the isohalines of 14 PSU and 17 PSU are shown over the SPM satellite field. These tracers indicate the spreading of the Danube's plume over the Western Black Sea, showing broad agreement in terms of extent and direction. The isohaline from both experiments shows small differences in the SSS field due the contribution of the river outlets.

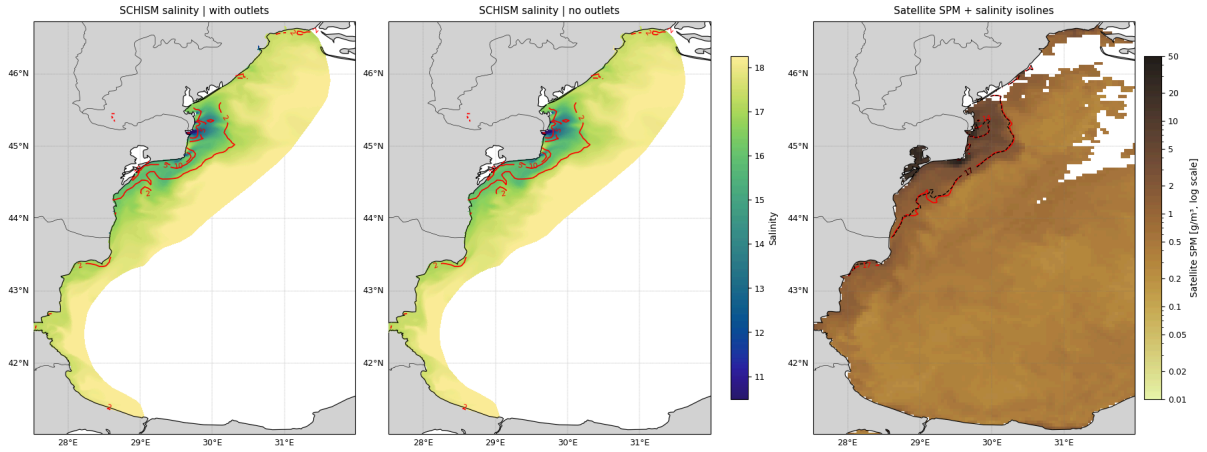


Figure 2.7.2 - Comparison of SSS between GCOAST-BS and SPM satellite fields for 2021.11.22. In the two first maps, isolines indicate the SPM values from satellite in g/m3 (red line). In the third map, the isohalines indicate SCHISM results (red line - with outlets; black line - no outlets) over the SPM satellite field.

The results show good performance for the representation of the LoC in the Northwestern Black Sea, including the spatial gradients and influence of the Danube's plume from the north to the south sectors.

3.5.1 Future Recommendations

Future recommendations may focus on an improved connection between E-HYPE and the coast. This implies the identification of the rivers with a permanent connection to the sea.

3.6 German Bight Coastal System

Here, additionally further analysis on the large-scale performance of the GCOAST-GB is investigated through comparison with remote sensing data. SSS and SST fields from the SCHISM model are compared with SST from the CMEMS product CMEMS_OBS-SST_BAL_PHY-TEMP_MY_L4_P1D-M, and SPM from the CMEMS product OBS-OC_GLO_BGC-TRANSP_MY_L3-MULTI-4KM_P1D.

Figure 3.6.1 compares the daily mean SST fields from GCOAST-GB, forced with the Reference and E-HYPE river discharge datasets against a satellite-derived SST analysis for 1 March 2017. The only difference between the two SCHISM simulations is the river volume discharge, while river temperature forcing remains identical in both cases.

Overall, the satellite SST analysis does not show a pronounced river plume signature. However, a cold-water feature west of the North Frisian Islands and in the Eider Estuary region (up to approximately 2°C colder; purple shading) is consistently represented in both the observations and the model simulations. In contrast, both simulations exhibit a distinct cold signal associated with the Elbe River that is not clearly evident in the satellite analysis. This discrepancy suggests that the river boundary conditions could be improved by coupling the E-HYPE discharge forcing with a corresponding river temperature forcing, which may lead to a more realistic representation of river-induced SST patterns.

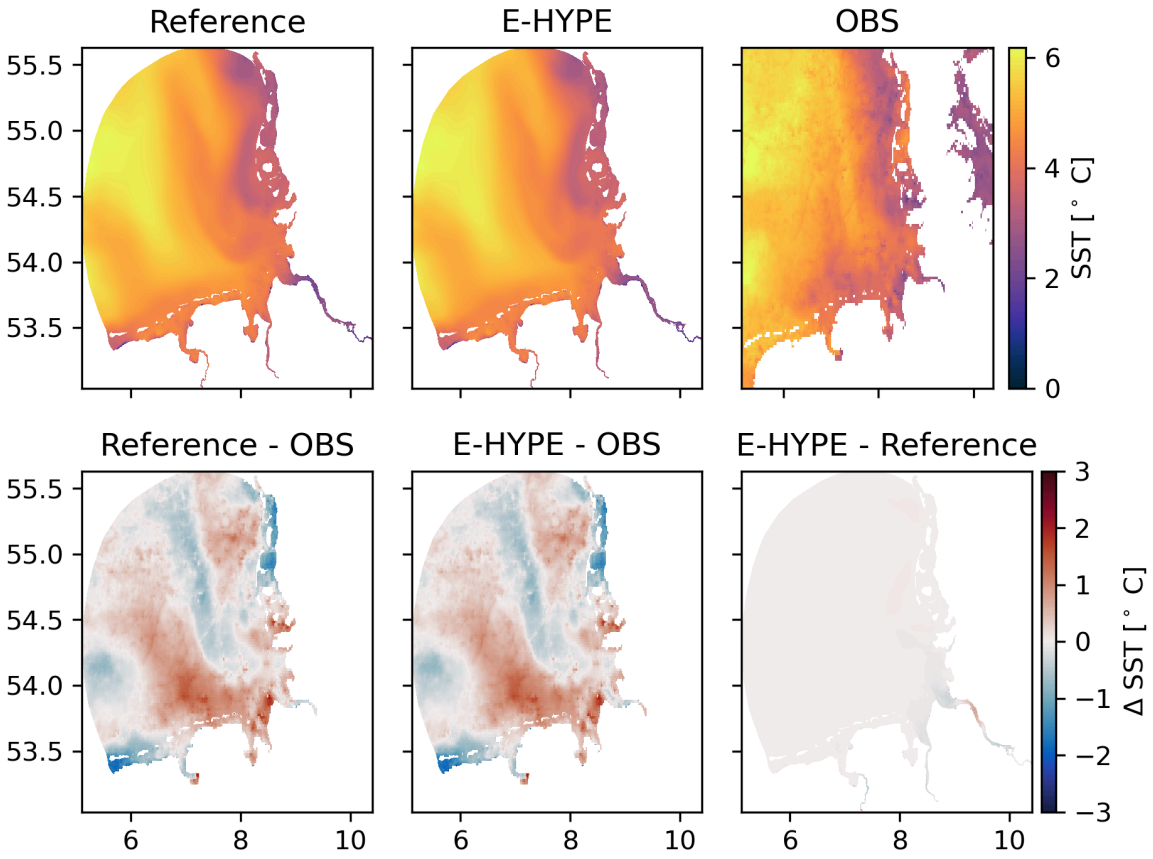


Figure 3.6.1 - Comparison of SST fields from the GCOAST-GB experiments and satellite observations on 1 March 2017. The upper panels show the daily mean SST fields for the SCHISM simulations forced with historic river discharge (left) and E-HYPE river discharge (center), as well as the satellite-based SST analysis product (right). The only difference between the two model simulations is the river volume discharge; river temperature forcing is identical in both cases. The lower panels show the SST differences between the model results and the satellite

observations for the historic (left) and E-HYPE (center) simulations, while the right panel shows the difference between the two model simulations.

Figure 3.62 compares SSS from GCOAST-GB with satellite-derived SPM for 23 March 2017, a day with the best satellite coverage during the month. Due to limited coastal resolution, estuarine and nearshore areas are only partially resolved in the satellite product.

The top panels show daily mean SSS from GCOAST-GB, forced by historical river runoff (left) and E-HYPE discharge (right). Both panels are overlaid with satellite-derived SPM isolines at 5 g m^{-3} (black) and 15 g m^{-3} (magenta). While estuarine salinity gradients are not directly traceable in the SPM field—likely due to limited nearshore coverage and resolution—a general offshore decrease is evident, broadly consistent with bathymetric zoning (approximately the 25–30 m depth contour) and the transition from regions of freshwater influence (ROFI) to offshore oceanic waters. The 15 g m^{-3} isoline broadly aligns with the 25–30 psu transition zone, marking the region where ROFI mixes with oceanic waters.

In the bottom panels, inversely the SPM field is depicted (on a logarithmic scale) with GCOAST-GB salinity isolines at 33 psu, 31 psu, and 20 psu. The 31 psu isoline broadly marks the boundary between higher coastal sediment concentrations and offshore waters, indicating reasonable agreement between the simulated salinity structure and observed sediment distribution at larger scales. This is most noticeable by the convex segment of the 31 psu line at about 54.5°N and the higher concentrations to the east of it. This pattern is qualitatively the same for the historical Reference and E-HYPE forced runs, yet a comparably stronger river discharges yields in lower SSS in the E-HYPE forced run in the mouth area and oceanward plume reach from the Weser and Elbe rivers.

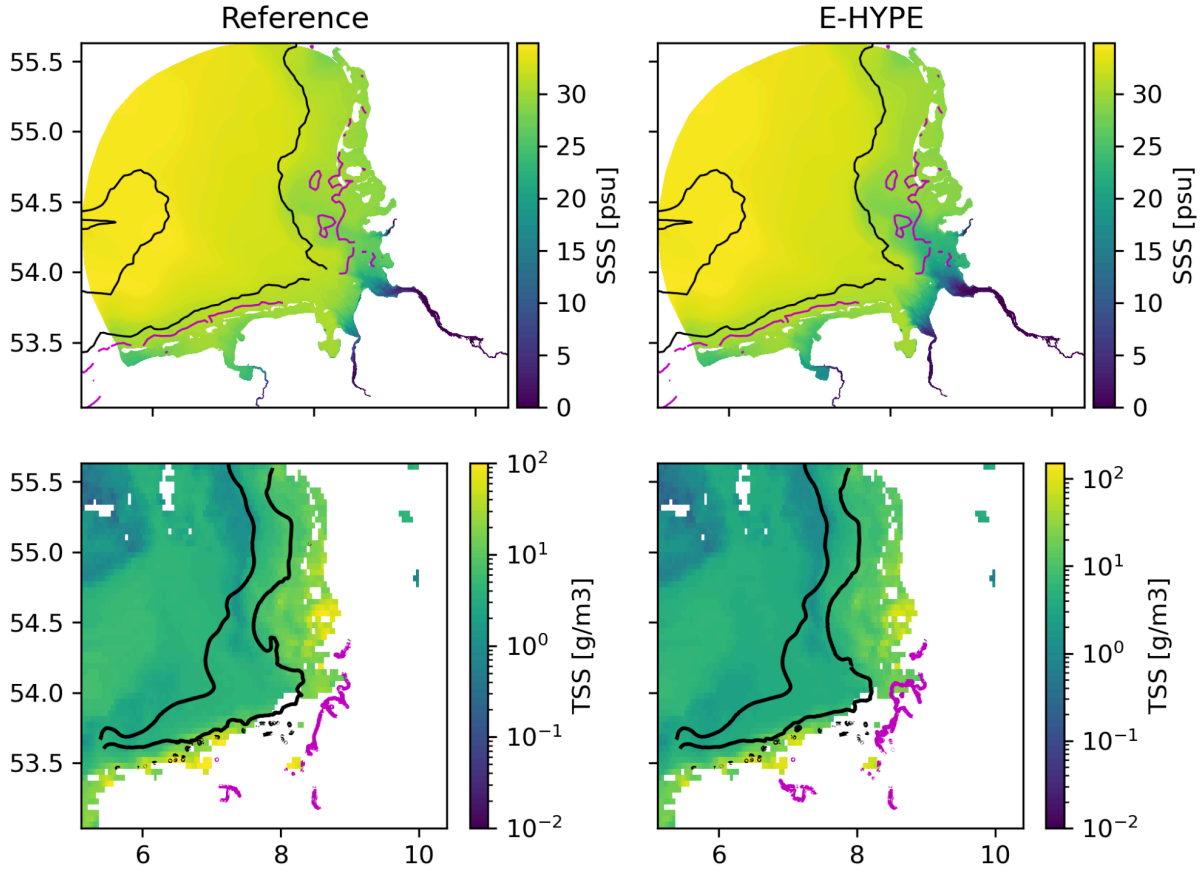


Figure 3.6.2 - Comparison of SSS from GCOAST-GB and satellite-derived SPM fields on 23 March 2017. The top panels show the daily mean SSS simulated by GCOAST-GB on 23 March 2017, forced with historical runoff (left) and forced with E-HYPE discharge (right) inflows. Both panels are overlaid with satellite-derived SPM isolines at 5 g m^{-3} (black) and 15 g m^{-3} (magenta). The bottom panels display the same satellite-derived SPM field on a logarithmic color scale. Overlaid are GCOAST-GB salinity isolines at 33 psu (black), 31 psu (black), and 20 psu (magenta). The contours in the left and right panels are derived from the reference and E-HYPE-forced simulations shown in the upper-left and upper-right panels, respectively.

3.6.1 Future Recommendations

As a future recommendation, we would also attribute the inclusion of temperature in E-HYPE data at the specific outlet as highly valuable.

3.7 Danish Sea Coastal System

Denmark's coastline is about 8000 km long in the Baltic North Sea region, with a minimum EEZ-to-coastline ratio (about 8.4 km). This means that one needs very high resolution to resolve local coastal topography. The current Danish Coastal Forecasting System is a Baltic-North Sea configuration with a focus on Danish waters, including seven two-way nested sub-domains among which three of them resolve important fjord domains with a resolution up to 0.1 nm. The connection to land is resolved by the riverine forcing of fresh water and pollutant fluxes, provided by E-HYPE. This approach resolves source-to-sea water and pollutant transport seamlessly. In the FOCCUS project, DMI further enhances resolution in the fjord and river mouth to 50 m. In this way, even part of the rivers are resolved by a 3D numerical model. This demonstration is given in section 2.6. Future improvements can be made by including the usage of water temperature from E-HYPE in HBM.

4. Conclusions

The present report has presented the final results of implementing the LoC interfaces within the seamless modeling framework developed for all the study sites. Through the varied coupling strategies and modeling techniques, the report (together with previous WP5 deliverables) demonstrates that seamless LoC modeling techniques provides a robust and transferable framework for better representing the river-sea interactions across a wide range of European coastal environments. Although the individual study sites differ in terms of hydrology, morphology, tidal forcing and hydrodynamics in general, the common outcome is that a more realistic freshwater forcing can enhance the simulation of coastal processes that are directly relevant to regional models and to improve operational forecasting systems.

The final findings from each case study are presented throughout this report, while the complete methodological developments are described in the WP4 deliverables, and the validation of the modelling frameworks is detailed also in the previous WP5 deliverables (D5.1, D5.2, and D5.3). Despite the different approaches implemented, some important common conclusions emerge from these WP5 findings. First, all case studies demonstrate that an accurate representation of river discharge is a key requirement for realistically reproducing coastal salinity patterns, freshwater plumes, and the associated physical processes at the LoC. Second, the coupling strategies developed along with the FOCCUS project consistently show added value during periods of strong riverine forcing, exactly when standalone marine models often are more likely to underestimate the spatial

extent and intensity of freshwater influence. Finally, the results show that there is not a unique and generally optimal coupling strategy that can be implemented for all coastal areas. Instead, the most effective modelling approach depends on the hydrodynamic characteristics and operational requirements of each system. While this highlights the need for site-specific adaptation when transferring seamless modelling approaches to different regions, it also demonstrates the importance of keeping a flexible modelling framework capable of accommodating diverse operational constraints within a consistent scientific methodology.

In addition to these common conclusions, WP4 and WP5 generated important site-specific lessons that provide valuable guidance for future seamless modelling developments. For the Portuguese coast, for example, the results showed that the main limitation of the 3D implementation lies in the representation of estuarine processes rather than in the EE methodology itself. This is an important finding as it confirms the robustness of the emulator approach while identifying the estuarine setup as the key area for further improvement. The study developed for the Dutch Continental Shelf demonstrates that, more important than the version of the hydrological model implemented, the use of such a model offers the possibility of integration of a hydrological modelling framework capable of generating consistent historical reconstructions and future scenario simulations, overcoming the limitations of gap-filled observational datasets. For the Adriatic Sea, the work done demonstrated that two-way online coupling with the EE substantially improves the representation of riverine inputs during high-discharge events, while also showing that increasing the spatial resolution of the regional model domain alone can be sufficient to reproduce much of the salinity variability associated with river discharge under less extreme conditions. Although these findings are specific to each study area, together they provide practical guidance on the strengths, limitations, and applicability of different seamless modelling strategies.

In this context, together with the methodological developments achieved in WP4, the work carried out within WP5 demonstrates that seamless LoC modelling frameworks are both scientifically robust and operationally relevant across a broad range of European coastal environments. These results highlight the potential of seamless modelling to support the evolution of Copernicus Marine Services and other future coastal forecasting systems by improving the representation of LoC interactions and their influence on coastal dynamics. Together, the methodologies developed in WP4 and validated through WP5 provide a solid basis for the downstream activities of WP9, where these advances will be integrated into the broader FOCCUS service framework. The implementation of more realistic

river and estuarine boundary conditions is expected to enhance the accuracy and reliability of modeling frameworks in general, including operational coastal forecasts, while also establishing a strong basis for the development of future operational services, early warning systems, and climate-oriented applications beyond the lifetime of the FOCCUS project.

5. References

Stolte, W. (2023). North Sea and Wadden Sea model validation database at Deltares. Retrieved from https://wstolte.github.io/nwdm/

Toffolon, M., & Piccolroaz, S. (2015). A hybrid model for river water temperature as a function of air temperature and discharge. Environmental Research Letters, 10, 114011. https://doi.org/10.1088/1748-9326/10/11/114011

van Leeuwen, S. (2024). EMORID riverine database (Version 4.0) [Dataset]. NIOZ. https://doi.org/10.25850/nioz/7b.b.th

Verri, G., Pinardi, N., Bryan, F., Tseng, Y.-H., Coppini, G., & Clementi, E. (2020). A box model to represent estuarine dynamics in mesoscale resolution ocean models. Ocean Modelling, 148, 101587. https://doi.org/10.1016/j.ocemod.2020.101587

Verri, G., Mahmoudi Kurdistani, S., Coppini, G., & Valentini, A. (2021). Recent advances of a box model to represent estuarine dynamics: Time-variable estuary length and eddy diffusivity. Journal of Advances in Modeling Earth Systems, 13, e2020MS002276. https://doi.org/10.1029/2020MS002276

Vilmin, L., Heye, S., Di Paola, F., & Blauw, A. (2026). 3D DCSM-FM with water quality: Model set-up and validation (Report No. 11211532-003-ZKS-0003, Version 1.1). Deltares. https://publications.deltares.nl/11211532_003_0003.pdf

6. Annex

Milestone 5.1 Summary:

Milestone MS5.1: Validation of regional hydrological and EBM model products was delivered in M27, as part of WP5. A summary of this document can be found below, as it is not available on the EU Portal or for public dissemination. Additionally, as commented in the submission of this milestone in the EU Portal, the Commission has the right to request access to this document directly using the project's shared drive here: https://drive.google.com/file/d/1Qr8Wcn0pDLL5xk9wg8dJ-3POBpSyX3Mn/view?usp=sharing (last access 30 July 2026).

This milestone covers Task 5.1 within WP5: Implementation of improved model systems for hydrology, estuary systems, which includes the subtasks:

- Evaluate and tune freshwater inputs towards improved model performance at coastal outlets, i.e., minimize model bias using ML methods to post-process WP4 data using available observations
- Compare European-scale freshwater inputs with regional hydrological models WRF-HYDRO (Adriatic Basin), MOHID Land (Western Iberia) and validate with relevant EO and in situ data coming from WP2-3 (e.g., EMODnet NRT observed data)
- Evaluate the improved EBM in selected estuaries to provide best estimations for coastal models using relevant EO and in situ data coming from WP2-3 (e.g., EMODnet NRT observed data)

Evaluation and tuning of freshwater inputs is reported within Deliverable 5.1 (D5.1) along with comparison of regional and continental-scale hydrological models, and with the datasets described in D5.2. Regarding hydrological models this milestone MS5.1 summarises key findings and validation results of regional (MOHID-Land and WRF-Hydro) and continental scale (HYPE and LISFLOOD+GREEN) hydrological models in order to provide conclusions about particularities of implementation of different hydrological models.

To achieve a well-trained Estuary Emulator (EE), and to address the scarcity of in situ measurements along fresh water domains, a dataset created using a high-resolution 3D finite element model (SHYFEM-MPI Z*) was used for the training phase. This dataset has been validated, and the corresponding results are documented in D5.3. The main focus of MS5.1 is the evaluation of the enhanced EE as a key step toward the development of a land-ocean continuum (LoC) modeling framework. This Milestone is:

- part of D5.3 and it describes work setup and main achievements on the Estuary Emulator validation and testing
- a summary of D5.1, it includes extended and updated results on hydrological model comparison